Probes of Structural and Electronic Environments of Phosphor Activators: Mössbauer and Raman Spectroscopy

Jack Silver* and Robert Withnall*

Center for Phosphors and Display Materials, University of Greenwich, Central Avenue, Chatham Maritime, Kent ME4 4TB, U.K.

Received March 13, 2003

Contents

1. General Introduction 2833
2. Mössbauer Spectroscopy 2834
2.1. Historical Background 2834
2.2. Iron 2835
2.2.1. Introduction 2835
2.2.2. Principles and Properties of ^{57}Fe Mössbauer Spectroscopy 2835
2.2.3. Chemical Properties 2835
2.2.4. Studies on Fe^{3+}-Containing Phosphors 2835
2.3. Gold 2835
2.3.1. Introduction 2835
2.3.2. Principles and Properties of ^{97}Au Mössbauer Spectroscopy 2836
2.3.3. Chemical Properties 2836
2.4. Europium 2836
2.4.1. Introduction 2836
2.4.2. Principles and Properties of ^{151}Eu Mössbauer Spectroscopy 2836
2.4.3. Chemical Properties 2836
2.4.4. Studies on Eu^{3+}-Containing Phosphors 2837
2.5. Tin 2838
2.5.1. Introduction 2838
2.5.2. Principles and Properties of ^{119}Sn Mössbauer Spectroscopy 2838
2.5.3. Chemical Properties 2838
2.6. Antimony 2839
2.6.1. Introduction 2839
2.6.2. Principles and Properties of ^{121}Sb Mössbauer Spectroscopy 2839
2.6.3. Chemical Properties 2839
2.6.4. Studies on Sb^{3+}-Containing Phosphors 2839
2.7. Zinc 2839
2.7.1. Introduction 2839
2.7.2. Principles and Properties of ^{67}Zn Mössbauer Spectroscopy 2839
2.7.3. Chemical Properties 2840
2.8. Gadolinium 2840
2.8.1. Introduction 2840
2.8.2. Principles and Properties of ^{155}Gd Mössbauer Spectroscopy 2840
2.8.3. Chemical Properties 2840
2.9. Other Rare-Earth Elements 2840
2.9.1. Dysprosium 2841
2.9.2. Erbium 2841
2.9.3. Thulium 2841
2.9.4. Ytterbium 2841
3. Raman Spectroscopy 2841
3.1. Historical Background 2841
3.2. Vibrational Raman Spectroscopy 2841
3.2.1. Introduction 2841
3.2.2. Oxides MO 2841
3.2.3. Oxides M_2O_3 2842
3.2.4. Oxides AB_xO_4 2844
3.2.5. Metal Sulfides (MS) 2845
3.2.6. Metal Oxysulfides (M_2O_2S) 2845
3.3. Electronic Raman Spectroscopy 2846
3.3.1. Introduction 2846
3.3.2. Phosphors Containing Ce^{3+} 2847
3.3.3. Phosphors Containing Eu^{3+} 2848
3.3.4. Phosphors Containing Tb^{3+} 2848
3.3.5. Phosphors Containing Yb^{3+} 2848
4. Studies Combining the Use of Mössbauer and Raman Spectroscopies 2849
5. Studies Combining the Use of Mössbauer and Luminescence Spectroscopies 2851
6. Conclusions 2852
7. Acknowledgments 2852
8. References 2852

* Address correspondence to either author. Tel.: +44 20 8331 8673. Fax: +44 20 8331 8405. E-mail: J.Silver@gre.ac.uk; R.Withnall@gre.ac.uk.

1. General Introduction

In this review we discuss two spectroscopic techniques that are very sensitive to low concentrations of activators (or in some cases quenchers) in phosphor lattices. A combination of Mössbauer and laser Raman spectroscopic techniques can give information on the valence state, spin state (where relevant), electronic environment, coordination number, crystallographic site, and emission spectra (both Stokes and anti-Stokes) of a range of important activators in phosphor materials, and can even tell if more than one valence state is present.

We will first review the phosphor literature of each of these spectroscopies separately, indicating both what has been done and what opportunities are available for future research.

In the final section we will illustrate what can be achieved by using both techniques on the same materials.

10.1021/cr0203544 CCC: $48.50
Published on Web 05/15/2004

Jack Silver was born in Sunderland, England, in 1948. He received his B.Sc. degree from the University of London in1970, and his Ph.D. from the University of London in1973, with John Donaldson. After 2 years of postdoctoral work at the University of London, he became a temporary Lecturer at the University of Birmingham, and then he was appointed to Inorganic Lectureships at the University of West Indies, Trinidad, in 1976, and subsequently at the University of Essex in 1978. He received his D.Sc. from the University of London in1992, and was appointed to a Readership at the University of Essex in the same year. In 1996, he was appointed to a full Professorship at the University of Greenwich and became Head of the Phosphor Group. He was chairman of the RSC Mössbauer Group from 1996 to 2001. His research interests include fundamental aspects of inorganic chemistry and light-emitting materials and the technological applications of phosphors.

Robert Withnall was born in Wednesbury, England, in 1958. He received his B.A. degree from Jesus College, Cambridge, in 1980, his M.Sc. degree in chemical spectroscopy from the University of East Anglia in 1981, and his Ph.D. from the University of East Anglia in 1984, with John Sodeau. He carried out postdoctoral research at the University of Virginia, with Lester Andrews, from 1984 to 1987, and was awarded the Sigma Xi Visiting Scientist award in 1987. He did further postdoctoral studies at the University of California, with Ara Apkarian, and at University College London, with Robin Clark. He was appointed to a Senior Lectureship in Inorganic/Physical Chemistry in 1993 at the University of Greenwich and became Reader in Materials in 2000. His research interests embrace fundamental aspects of inorganic and physical chemistry and applications and theoretical aspects of vibrational and electronic spectroscopy. He was appointed to an Adjunct Professorship in Chemistry at the University of Syracuse, New York, in 2002.

2. Mössbauer Spectroscopy

2.1. Historical Background

Rudolf Mössbauer[1,2] discovered the phenomenon of recoil-free nuclear resonance fluorescence some 45 years ago, and it is over 40 years since Kistner and Sunyar[3] reported the first indications of hyperfine interactions in a chemical compound. Mössbauer spectroscopy has matured into a useful laboratory technique that, although not universally available, through collaboration is widely used in the study of chemical, metallurgical, geochemical, industrial, and biological materials. However, the use made of this powerful technique by phosphor chemists has been rather limited, so it is hoped that this review will stimulate its use in this field.

Many books and reviews have discussed the basic principles of the technique and related the origin and derivation of the hyperfine interactions that can be used to derive chemical information from Mössbauer spectra. In this review the authors will therefore not cover any of the above details but simply refer the reader to a number of the many textbooks on the subject.[4−12]

There have been, over the years since its discovery, many papers devoted to the study of many of the lattices used as host lattices (by phosphor chemists) for reasons other than phosphor research. For this reason the background research and Mössbauer spectra are often already in the literature. Indeed, in the case of europium compounds, a large number of materials relevant to the preparation and manufacture of phosphors were already well studied within the first few years of the development of the technique. It is the purpose of this section of the review not to try to list all of these works but to give an overview of the major work carried out on the more commonly available elements to which Mössbauer spectroscopy can be routinely applied and that have relevance to phosphor research. These elements are iron, gold, europium, tin, and antimony. Less commonly available elements that have been shown to be amenable to Mössbauer spectroscopic investigation include zinc, gadolinium, dysprosium, erbium, and thulium.

The hyperfine parameters that will be concentrated herein are the chemical isomer shift (δ) and the quadrupole splitting (ΔE_Q). The former provides information about s electron density at the nucleus and the latter details of the asymmetry of the electronic environment around the Mössbauer atom. In addition, magnetic relaxation effects will be shown to be useful to follow diffusion of phosphor activators in lattices.

The fact that, for lattices that are appreciably ionic, a reasonable Mössbauer spectrum for metals that are present around ca. 1.0% or greater would be expected means that, for most activators that are Mössbauer active, the δ value should be indicative of valence state. This is particularly true for oxide, fluoride, or oxyhalide lattices, which for transition metals will cause high-spin environments. For main block elements and rare-earth elements, it would be expected that the δ value would easily give the valence state. The valence states of elements can be very important, as transition elements that have partly filled d electron shells (other than Mn^{2+}, Fe^{3+}), i.e., Ti^{3+}, V^{3+}, Cr^{3+}, Fe^{2+}, Co^{2+}, Ni^{2+}, and Cu^{2+} (all known as quenchers or activators (for some of them) of luminescence), cannot undergo an excitation transition because of ground-state coupling to the local phonon modes, which results in the emission of infrared

radiation.[13] Hence, to be able to tell the difference between the presence of high-spin iron(III) and high-spin iron(II) (the former can be an activator) is important, as the latter can dissipate excitation energy to the lattice by phonon processes.

The next section details some of the more commonly available Mössbauer isotopes, with comments on studies or potential studies of possible interest to phosphor chemists.

2.2. Iron

2.2.1. Introduction

The ease of measurement of ^{57}Fe Mössbauer spectra (14.41 keV gamma energy) has resulted in very widespread use of this technique to probe iron-containing solid-state materials. ^{57}Fe has a natural abundance of 2%, and this is usually good enough to study normal iron compounds. However, where iron is present in very small amounts, such as in biological materials or in phosphors, where it is used as an activator or a killer, it may be necessary to prepare the sample with 96% ^{57}Fe-enriched iron to facilitate Mössbauer investigations.

2.2.2. Principles and Properties of ^{57}Fe Mössbauer Spectroscopy

^{57}Fe Mössbauer spectroscopy is a marvelous method to probe and investigate the stereochemistry of and bonding in inorganic iron compounds in the solid state. The source used for ^{57}Fe is ^{57}Co (the half-life of 270 days is conveniently large). The ^{57}Co is usually embedded in a metal matrix such as rhodium or platinum by electrolytic deposition and subsequent diffusion by annealing. The ^{57}Co is manufactured by the (d,n) reaction on ^{56}Fe (91.5% abundant in natural iron) in a cyclotron. The gamma energy is relatively low so that recoil effects are small. Thus, the Mössbauer spectra of iron-containing phosphors should be able to be recorded easily in the temperature range of 0−400 K or even at higher temperatures (so long as 90% or better enriched ^{57}Fe is used in the phosphor preparation).

The nuclear spin states of ^{57}Fe are $^1/_2$ (ground state) and $^3/_2$ (excited state); thus, the Mössbauer spectra manifest quadrupole-split doublets or simple singlets. The natural line width of ^{57}Fe is about 0.19 mm s^{-1}, which facilitates ready resolution.

The magnetic moments of the two states are of suitable magnitude so as to allow the use of magnetic perturbation methods for the determination of the sign of the field gradient, should it be required. For most purposes the two most important Mössbauer parameters for iron are the δ and ΔE_Q values. ^{57}Fe δ values are usually quoted relative to natural iron.

2.2.3. Chemical Properties

Chemical isomer shift (δ) values are dependent on the s electron density at the iron nucleus relative to a reference material (usually natural Fe). As the s electron density in the iron nucleus is related to the valence shell of the atom, then factors that effect the latter will also influence the former. Therefore, p and d electron shielding will directly affect the δ value.

Table 1. Mössbauer Parameters for Octahedral High-Spin Iron(III) Halides and Oxides

	T (K)	δ (mm s^{-1})[a]	ΔE_Q (mm s^{-1})	ref
FeF_3	296.5	0.489		14
$FeF_3 \cdot 3H_2O$	rt	0.445	1.48	15
$FeCl_3$	rt	0.436		16
$FeCl_3 \cdot 6H_2O$	300	0.45	0.97	16
$FeBr_3$	78	0.55		17
K_3FeF_6	rt	0.42	0.38	15
α-Fe_2O_3	298	0.38	0.12	18
γ-Fe_2O_3	rt	0.27 0.41		19

[a] Relative to natural Fe.

Table 2. Mössbauer Parameters for Octahedral High-Spin Iron(II) Halides and Oxides

	T (K)	δ (mm s^{-1})[a]	ΔE_Q (mm s^{-1})	ref
FeF_2	298	1.37	2.79	20
$KFeF_3$	rt	1.33	0.0	21
$KFeF_3$	rt	1.30	0.0	22
$FeCl_2$	78	10.97	0.895	23
$FeCl_2 \cdot H_2O$	rt	1.13	2.03	24
$FeCl_2 \cdot 2H_2O$	298	1.03	2.50	25
$FeCl_2 \cdot 4H_2O$	rt	1.221	2.984	26
$FeBr_2$	78	1.34	1.043	23
$FeBr_2 \cdot H_2O$	rt	1.14	2.49	24
$FeBr_2 \cdot 4H_2O$	rt	1.22	2.83	24
FeI_2	78	0.802	0.93	23
$Fe_{0.93}O$	297	0.91 0.86	0.46 0.78	27

[a] Relative to natural Fe.

The values of some high-spin iron(III) halides[14−17] and oxides[18,19] that fall in the range 0.27−0.55 mm s^{-1} are given in Table 1, whereas those of high-spin iron(II) are in the range 0.8−1.4 mm s^{-1} and are presented in Table 2.[20−27] Clearly, it is easy to distinguish between these valence states, and impurities of iron(II) in iron(III)-activated phosphors could easily be identified. In addition, iron(II) ΔE_Q values tend to be much larger than those of similar iron(III) compounds.

2.2.4. Studies on Fe^{3+}-Containing Phosphors

A recent ^{57}Mössbauer spectroscopic study of the infrared-emitting phosphor $LiAlO_2$:Fe (prepared with 0.1 mol % ^{57}Fe) was used to show how the final annealing of the sample led to a more even distribution of the Fe^{3+} activator.[28] This was seen by comparing the paramagnetic relaxation spectra before and after final annealing. The final spectrum showed evidence of increased magnetic dilution. The sample at this stage also manifested an increase in the photoluminescence efficiency. It is believed that this is the first time a more homogeneous activator distribution (proven from the Mössbauer spectra) has been shown to improve luminescence directly. That is, instead of the improvement of homogeneity of activator distribution being inferred from the increase in emission efficiency.[28]

2.3. Gold

2.3.1. Introduction

The high gamma energy of ^{197}Au (77.3 keV) leads to low recoil-free fractions, and it is therefore usual

to immerse both the source and the absorber in liquid nitrogen. When recording Mössbauer spectrum at such temperatures, it must be realized that the structures can undergo phase changes between 4.2 K and room temperature. This means that information gained from Mössbauer parameters taken at 4.2 K may not be directly relevant to phosphor behavior at room temperature.

2.3.2. Principles and Properties of ^{97}Au Mössbauer Spectroscopy

The Mössbauer-active isotope of gold is ^{97}Au, which has a 100% natural abundance. The spin states of ^{197}Au are $^3/_2$ (ground state) and $^1/_2$ (excited state); therefore, Mössbauer spectra are simple quadrupole doublets. The natural line width is 0.94 mm s^{-1}. This leads to experimental line widths (source and absorber) of about 1.9 mm s^{-1}, and as the ranges of δ and ΔE_Q values are large, the spectra are therefore well resolved.

However, magnetic splittings for ^{197}Au are small compared to the line width, and massive fields (of around 100 T) are necessary if good spectra are required. Clearly such fields are beyond the range of most laboratory magnets.

Sources for ^{197}Au are usually natural or enriched platinum foils, which can be irradiated in a nuclear reactor and turned into useable sources. ^{197}Pt has a half-life of 18 h, and this means sources can be used for 4−5 days and then reactivated as needed.

2.3.3. Chemical Properties

The δ values for ^{197}Au have been shown to be very sensitive to chemical environment, and they are usually referenced to elemental gold.[29]

Au(I) is the only oxidation state of Au that can be used as an activator in phosphors. Au(II) would be expected to act as a quencher of luminescence if it could be stabilized in phosphor lattices, as would Au(III).

Although many compounds have empirical formulas that might be expected to be Au(II) compounds, they are in fact mixed-valence systems involving Au(I) and Au(III).[29] In other examples, the presence of metal−metal bonding increases the effective covalency of the gold to 3+.[29] Recently asymmetric mono- and dications of Au(II) organometallic complexes have been reported,[30] but there has been no finding of this valence state in oxide, halide, or sulfide lattices. Hence, in this work we will consider only Au(I).

In the Au(I) oxidation state, the gold atoms have a 5d^{10} electron configuration; thus, no problems arise from nonbonding electrons. In Au(I) coordination compounds, the usual stereochemistry is linear (two-coordinate Au atoms), but instances of three and four coordination have been reported.[31] The different coordination numbers are easily distinguished from the Mössbauer parameters.

Parish and co-workers[29,32−34] along with others[35,36] have shown good correlations between δ and ΔE_Q values for Au(I) compounds in different coordination environments,[29] building on earlier findings.[37−39]

Table 3. ^{151}Eu Mössbauer Parameters for (a) Eu^{3+} and (b) Eu^{2+} Halides and Oxides

(a) Eu^{3+} Halides and Oxides

Eu^{3+} compound	T (K)	δ (mm s^{-1})[a]	ref
EuF_3	rt	0 (standard)	40
$EuCl_3$	rt	+0.08(9)	40, 41
$EuBr_3$	rt	+0.31(5)	40
EuI_3	rt	+0.31(4)	40
EuOF	rt	−0.35(2)	40
EuOCl	rt	−0.06(4)	40
Eu_2O_3 (cubic)	rt	+1.037	40, 42, 43

(b) Eu^{2+} Halides and Oxides

Eu^{2+} compound	T (K)	δ (mm s^{-1})[a]	ref
EuF_2	rt	−14.00	40, 44−46
$EuCl_2$	rt	−13.103	40, 47−49
$EuBr_2$	rt	−13.43	40, 45
EuI_2	rt	−12.50	46−48, 50
EuO	rt	−12.28	40, 47, 51

[a] Relative to EuF_3.

There have as yet been no studies using ^{197}Au Mössbauer spectroscopy specifically aimed at phosphor materials.

2.4. Europium

2.4.1. Introduction

Europium has two isotopes that can be used for Mössbauer spectroscopy: ^{151}Eu (47.8%) and ^{153}Eu (52.18%). However, the energy of the Mössbauer γ-ray for ^{151}Eu is 21.54 keV, and it is therefore more convenient to use this isotope. It is apparent in Table 3 that there are large differences between the δ values of Eu^{2+} and Eu^{3+} compounds; thus, these oxidation states are easy to assign.[40−51]

2.4.2. Principles and Properties of ^{151}Eu Mössbauer Spectroscopy

The gamma energy in ^{151}Eu Mössbauer spectroscopy is 21.54 keV, and the transition takes place between $^5/_2$ (ground-state nuclear spin) and $^7/_2$ (excited-state nuclear spin). The source is ^{151}Sm (its half-life is 90 y). $^{151}SmF_3$ has a good recoil-free fraction, 0.485 at 300 K, and a small line width, 2.52 mm s^{-1}.[42] This makes it a convenient source. Europium δ values measurements are usually referenced to Eu_2O_3 or EuF_3, but the latter are now preferred. The difference between the δ values of Eu_2O_3 and EuF_3 is 1.037 ± 0.013 mm s^{-1} for the δ value of cubic Eu_2O_3 relative to EuF_3.[40,52] All shifts given in Table 3 are converted by adding 1.037 mm s^{-1} to the original data; this table summarizes the evaluation of the literature data for the given references.[40−51]

2.4.3. Chemical Properties

It is difficult, however, to measure ΔE_Q values in Eu compounds due to the electronic configurations of Eu^{3+} and Eu^{2+}. For Eu^{3+} the configuration is 4f^6, which has a ground state of ^7F_o which has a zero total angular momentum. In the case of the Eu^{2+} ion, a 4f^7 half-filled shell is found for the ion in its $^8S_{7/2}$ ground state, which does not generate a valence electron contribution to the electric field gradient.

Hence, any ΔE_Q value for Eu^{3+} and Eu^{2+} compounds can only arise from the lattice contributions to the electric field gradients and consequently would be expected to be small. In fact, any ΔE_Q values that occur are observed only as a slight broadening of the resonance line, and analysis is defied because of the large number of lines from the $^5/_2$, $^7/_2$ nucleus spin states. The presence of small ΔE_Q values may generate small errors in the δ values if the envelope is fitted as a single line.

Europium is used as an activator for phosphors in both the Eu^{3+} and Eu^{2+} valence states. The former is usually used to produce a red phosphor, as in the television phosphors Y_2O_3:Eu^{3+}, Y_2O_2S:Eu^{3+}, and YVO_4:Eu^{3+}, whereas Eu^{2+} is often used to produce green or blue phosphors. Hence, knowledge of which valence states of Eu are present in a phosphor can be very important. For instance, the presence of Eu^{3+} in an Eu^{2+} phosphor may lead to loss of excitation energy via undesired side reactions or emission.

A wide range of ternary and complex europium oxide lattices have been studied, and thus there is much Mössbauer spectroscopy literature with which similar studies on phosphor materials could be compared. Among the lattice types studied are perovskites,[53−60] pyrochlores,[61,62] garnets,[63−66] bronzes,[67−70] and others.[71−74]

2.4.4. Studies on Eu^{3+}-Containing Phosphors

The concentration-dependent site occupancy of the phosphor Y_2WO_6:Eu has been studied using ^{151}Eu Mössbauer spectroscopy.[75] From the crystal structure[76,77] it was established that there are three nonequivalent sites present. By assuming that the Eu^{3+} in Y_2WO_6 was scattered in these three sites, the Mössbauer spectra were fitted at first by constraining the sites and then letting them vary. Small differences in the covalency for the three sites are suggested from the observed δ values. It was shown that the relative occupancy of one of the sites was strongly dependent on the Eu^{3+} concentration.[75]

The possibility of using Mössbauer spectroscopy to investigate Eu^{2+}- and Eu^{3+}-activated phosphors to study the valence state of the activator and its position in the crystal lattice was reported in 1980.[78] The Eu^{3+} phosphors studied included $(Y_{1-x}Eu_x)_2O_3$ and $(Y_{1-x}Eu_x)(V_{1-y}P_y)O_4$. The δ values were shown to have a good correlation with lattice type. The δ values of the Eu^{3+} in Y_2O_3 are higher by 0.7−0.8 mm s^{-1} than those containing vanadate and phosphate. The Eu^{3+} is in six coordination in the former compound and in eight coordination in the latter case.

When $Ba_{0.9}Eu_{0.1}MgAl_{11}O_{19}$ was prepared at 1500 °C in air, it contained only Eu^{3+}. The isomer shift of the Eu^{3+} was less in the aluminate host than in either Y_2O_3 or $(Y_{1-x}Eu_x)(W_{1-y}P_y)O_4$. This was interpreted to mean that the electron density at the nucleus of Eu^{3+} is less in the ferrite-type structure than in the cubic or tetragonal structure. When $Ba_{0.9}Eu_{0.1}MgAl_{11}O_{19}$ was fired in a partial atmosphere of hydrogen, it was found that the atomic ratio of Mg and Eu in the samples has an effect on the Eu^{2+}:Eu^{3+} ratio.[78] The preliminary data reported in this paper show the direction of further experiments and the possibility to examine the details of the incorporation processes.

The structure, luminescence, and Mössbauer spectra of $EuVO_4$ in the Scheelite and zircon phases have been reported.[79] The Scheelite phase was stabilized by a high-pressure, high-temperature method and was transformed into a stable zircon phase by an annealing treatment in air. Scheelite $EuVO_4$ manifested strong emission at 617 nm (associated with the $^5D_0-^7F_2$ transition of Eu^{3+}). The Mössbauer parameters for this phase were $\delta = -0.55 \pm 0.01$ mm s^{-1} and $\Delta E_Q = -8.0 \pm 0.3$ mm s^{-1}, whereas those for the zircon phases are $\delta = -0.06 \pm 0.02$ mm s^{-1} and $\Delta E_Q = -8.6 \pm 0.3$ mm s^{-1}. The lower δ value recorded for the Scheelite phase is ascribed to a reduced covalency in the Eu−O bond originating from a charge transfer from oxygen to Eu^{3+}; this caused an enhanced shielding of 4f electrons in the s orbital as well as a decrease in s electron density around the Eu^{3+} nucleus.[79] We note that, unfortunately, this material cannot be described as a useful phosphor as too much Eu is present, but it does open the way for similar studies in $Y_{1-x}Eu_xVO_4$.

For the phosphor BaFBr:Eu, Mössbauer spectroscopic studies have shown that the coupling of phonons to the Eu^{2+} ion is greater than that between Eu^{3+} and phonons.[80] The study also indicates a temperature-dependent electron exchange between Eu^{2+} and Eu^{3+} sites in the BaFBr lattice.[80]

The Mössbauer spectra of a TiO_2:Eu sample containing 4 mol % Eu calcined over a range of temperatures from 300 to 1000 °C have been reported.[28] There is evidence from the line widths that the samples contain Eu^{3+} in more than one electronic environment. The temperature dependence of the line width was linked to the titania phases present in the X-ray powder diffraction data for each calcined sample. At 500 °C both brookite and anatase were present, but at higher temperatures the amount of brookite decreased, as did the halfwidth in the Mössbauer spectra. At 1000 °C the sample was pure rutile, the Mössbauer spectroscopic data showed a lower isomer shift, and a wider line width indicated more than one Eu^{3+} site in the lattice.[28]

The phosphor $BaMgAl_{10}O_{17}$:Eu^{2+} (BAM) is of current importance because of its use as the blue phosphor in fluorescent lamps and plasma television (TV). It has been stated that BAM:Eu^{2+} degrades more rapidly due to oxidation of Eu^{2+} from heat treatment in air during lamp processing.[81] This phosphor has been shown to deteriorate in plasma TVs, and increasing its maintenance would be a considerable advance.[82] A recent study of BAM using ^{151}Eu Mössbauer spectroscopy (at 4.2 K) has revealed a number of interesting findings.[83] The phosphor investigated contained about 10% Eu^{2+} in place of Ba^{2+}. The Mössbauer line shapes are reported to rule out a single substitutional site in BAM (though only one Ba site is reported in the crystal structure and the Eu^{2+} cations are thought to substitute on these sites). It is suggested that the line broadening observed could be either quadrupolar or magnetic in origin. However, the authors favor a quadrupolar interaction that fits to five Eu sites. They report three Eu^{2+} sites (see Table 4), an Eu^{3+} site, and a fifth site which is weakly populated and said to lie outside the

Table 4. ^{151}Eu Mössbauer Parameters for $BaMgAl_{10}O_{17}:Eu^{2+}$

δ (mm s^{-1})[a]	e^2qQ/h (MHz)[a]
−17.61	854.09
−14.25	−2499.52
−11.50	−1273.41
−8.69	−1020.07
−0.98	−1437.50

[a] From ref 83. Unfortunately, the authors do not give any idea of what the δ value are referenced to.

range of shifts for divalent and trivalent Eu. However, we do not agree with the last point made by the authors as the fifth site is close to the Eu^{2+} values, and similar δ values for Eu alloys[84] were ascribed by others[6] to Eu^{2+} configurations. Hence, we consider that there is evidence for four Eu^{2+} sites in the BAM sample investigated; however, the authors do not show the Mössbauer spectrum. The authors chose only to focus on the first three sites (in Table 4), which they ascribed to the three dominant Eu^{2+} sites in the lattice. They suggest that the three locations for Eu^{2+} cations are a Beevers−Ross site, a mid-oxygen site, and an anti-Beevers−Ross site. They admit that the nuclear quadrupole coupling constants they report are larger than any other data reported to date. However, this work shows that the europium ions in BAM:Eu^{2+} are distributed over more than one type of site.[83] The authors refer back to this work[83] in a further paper where BAM:Sm^{2+} is studied.[85] In the latter it is concluded that, as Eu^{2+} and Sm^{2+} possess nearly identical ionic radii and chemical properties, the results from the study on BAM:Sm^{2+} provide additional support for the "multiple sites" hypothesis for divalent ions in the phosphor.[86] It needs to be noted that a recent neutron diffraction study indicated that the Eu^{2+} ions were on a site close to the anti-Beevers−Ross site.[86] Two of the questions that are important in understanding the bulk structure and surface chemistry of BAM:Eu^{2+} have therefore been addressed by these investigations:[83,85]

(a) Where are the Eu^{2+} cations in the structure of BAM:Eu?

b) What is the fate of these Eu^{2+} cations in the phosphor when it is heated in air or used under ultraviolet and visible light?

However, the jury is still out on the answers.

2.5. Tin

2.5.1. Introduction

The fundamentals of ^{119}Sn Mössbauer spectroscopy were laid down over 35 years ago, and major reviews appeared about 30 years ago.[87,88] This means that, for the relatively few phosphors that depend on Sn(II) as an activator, there is a wealth of Mössbauer spectra to use as reference materials.

2.5.2. Principles and Properties of ^{119}Sn Mössbauer Spectroscopy

^{119}Sn Mössbauer spectroscopy is an easily interpreted probe for the stereochemistry and bonding in tin compounds.[89−91] The ^{119}Sn source (half-life 245 days) is made by neutron irradiation of ^{118}Sn in a suitable matrix such as $CaSnO_3$ or $BaSnO_3$. The gamma energy is relatively low (23.8keV) so that recoil effects are small, and thus Mössbauer spectra of inorganic lattices can readily be obtained at both liquid N_2 and room temperature.

Table 5. Mössbauer Parameters for (a) Tin(IV) and (b) Tin(II) Oxides and Halides

(a) Tin(IV) Oxides and Halides

tin(IV) compound	δ (mm s^{-1})[a]	ΔE_Q (mm s^{-1})	ref
SnF_4	−0.47	1.66	92
$SnCl_4$	+0.85	0	93
$SnCl_5{\cdot}5H_2O$	+0.25	0	93
$SnBr_4$	+1.15	0	93
SnI_4	+1.55	0	94
K_2SnF_6	−0.59	0	95
K_2SnCl_6	+0.45	0	96
K_2SnBr_6	+0.75	0	96

(b) Tin(II) Oxides and Halides

tin(II) compound	δ (mm s^{-1})[a]	ΔE_Q (mm s^{-1})	ref
SnF_2 (monoclinic)	3.60	1.80	97
$SnCl_2$	4.07	0	98
$SnBr_2$	3.93	0	98
SnI_2	3.85	0	98
$KSnF_3$	3.02	1.92	99
$KSnCl_3$	3.82	0.77	100
$KSnBr_3$	3.83	0	100
SnO black	2.71	1.45	101
SnO red	2.60	2.20	101

[a] Relative to SnO_2 (this is the 0.0 mm s^{-1} point on the δ scale for Sn compounds).

The spin states of ^{119}Sn are $^1/_2$ (ground state) and $^3/_2$ (excited state), and so the Mössbauer spectra are quadrupole-split doublets or simple singlets. In ^{119}Sn Mössbauer spectra, the presence of a ΔE_Q means that some kind of sp hybridization must be present. The ^{119}Sn natural line width is 0.62 mm s^{-1}, which allows reasonable resolution. ^{119}Sn δ values are usually quoted relative to SnO_2 or $BaSnO_3$ standard absorbers; these have identical δ values within experimental error.

The tin(II) and tin(IV) oxidation states in oxide and halide lattices are easily established from their δ values (Table 5).[92−101]

2.5.3. Chemical Properties

It is worth noting that Sn(II) phosphors are usually first fired in air and result in optically inert materials. However, if they are fired in reducing atmospheres, then the luminescence of the Sn(II) activation develops. The reason for this has been ascribed to the fact that most tin compounds are easily reduced to the metallic form. By first firing in air, the tin is incorporated within the host lattice in an optically inert form (i.e., as Sn(IV)). Refiring in a reducing atmosphere converts this to Sn(II), and the resulting phosphors have high-energy efficiencies and brightness. The emission color of Sn(II) has been shown to be dependent on the host lattice, and emission colors have been observed to change from the ultraviolet to the deep red. Table 6 presents the various effects that the crystal lattice parameters have upon both the intensity (energy efficiency) and the energy content (wavelength) of the emission bands.[13] We and others have explained the signifi-

Table 6. Emission Bands of Sn(II) in Alkaline Earth Pyrophosphate Lattices (Adapted from Ref 13)

lattice	cation radius	emission color	emission peak (nm)	relative intensity
α-$M_2P_2O_y$ (High-Temperature Form), Orthorhombic				
M=Ca	0.99	UV	362	17
		blue	429	15
M=Sr	1.13	blue	463	100
M=Ba[a]	1.35	deep-red	676	40
β-$M_2P_2O_7$ (Low-Temperature Form), Tetragonal				
M=Ca	0.99	UV	369	14
M=Sr	1.13	UV	364	80
M=Ba[a] (orthohombic)	1.35	green	505	65

[a] The crystal structure of the material is not yet established.

cance of the outer ns^2 electrons of low-valence p block elements to the population of the conduction bands and their role in luminescence.[102,103] Mössbauer spectroscopic studies of Sn(II) phosphors should yield more information on the role of the Sn $5s^2$ electrons in a similar way to early studies on colored Sn(II) oxides and halides.[104−122]

2.6. Antimony

2.6.1. Introduction

Although ^{121}Sb Mössbauer spectroscopy has attracted much interest in the past 35 years, it is not as widespread in use as that of ^{57}Fe or ^{119}Sn. The two main reasons for this are that first, as the Mössbauer gamma energy is 37.15 keV, both the source and the absorber usually require cooling, and second, the quadrupole splittings are usually less than the experimental line width. The natural abundance of ^{121}Sb is 57.25%, which means that it is rarely necessary to use isotope enrichment, even for dopant studies.

2.6.2. Principles and Properties of ^{121}Sb Mössbauer Spectroscopy

The 37.15-keV resonance of ^{121}Sb is populated directly with 100% efficiency by the β^- decay of ^{121}Sn, and the gamma is emitted via a transition from the $^7/_2$ excited state to the $^5/_2$ ground state of ^{121}Sb. The half-life of ^{121}Sn is 76 years, and it is therefore a convenient source. The most convenient source matrices are $^{121}SnO_2$, $Ba^{121}SnO_3$, and $Ca^{121}SnO_3$.[123]

In some conditions, quadrupole splittings have been observed in the ^{121}Sb resonance; however, as the line splitting is usually less than the experimental line width, this is not usually the case.

2.6.3. Chemical Properties

The chemical isomer shifts (δ values) are quite large in ^{121}Sb; from the extremes of Sb(III) to Sb(V) there is a range of ~21 mm s $^{-1}$.[124] Typical Sb(III) and Sb(V) δ values are given in Table 7.[125−128]

It is obvious that Sb(III) δ values are in the range from −16.5 to ~ −10.0 mm s^{-1}, whereas those for Sb(V) are in the range from ~4.2 to −3.5 mm s^{-1}. Therefore, for phosphors that are dependent on Sb(III) activators, any Sb(V) impurities will be easily seen by ^{121}Sb Mössbauer spectroscopy, and therefore this technique should be attractive to phosphor chemists.

Table 7. Mössbauer Parameters for (a) Sb(III) and (b) Sb(V) Oxides and Halides

(a) Sb(III) Oxides and Halides

Sb(III) compound	T (K)	Δ (mm s^{-1})[a]	ΔE_Q (mm s^{-1})	ref
Sb_2O_3 (cubic)	80	−10.4(3)		125
SbF_3	78	−14.6(2)	19.6(9)	126
$SbCl_3$	80	−15.5(2)		127
$SbBr_3$	80	−15.85(2)		127
SbI_3	80	−16.5(3)		127

(b) Sb(V) Oxides and Halides

Sb(V) compound	T (K)	Δ (mm s^{-1})[a]	ΔE_Q (mm s^{-1})	ref
Sb_2O_5	80	0.5(2)		125
SbF_5	80	+2.0(2)		125
$SbCl_5$	80	−3.5(3)		125
$KSbF_6$	4	+4.2(5)	8.0(1.6)	128

[a] Relative to $^{121}Sb/SnO_2$.

2.6.4. Studies on Sb^{3+}-Containing Phosphors

Surprisingly, there has been only one such investigation to date.[129] This paper dates back to 1975, and is a report of a Mössbauer spectroscopy study on the incorporation of Sb^{3+} into calcium halophosphate phosphors.[129] It presents evidence that the proportion of Sb(III) and Sb(V) in the lattices of fluorapatites and chlorapatites depends on the firing temperature (when fired in air). Surprisingly, less Sb(V) contamination was found at higher firing temperatures, but there is no mention of checking the phosphor properties. Therefore, it is not possible to conclude if the Sb(III) is all in one lattice site or in both, or in fact whether it has been first oxidized and partially reduced with some oxide ligands remaining in the lattice. The authors report different δ values of Sb(III) in two samples of fluorapatite fired under a nitrogen atmosphere. They also report different δ values for both Sb(III) and Sb(V) sites fired in air. Although they say that the least negative values of δ for the Sb(III) sites are found for chlorapatite samples and the most negative for fluorapatite samples, they do not make detailed conclusions on the interpretation. They stated that more conclusions would follow in a later work, which does not appear to have been published. Indeed, in 1980, the initial work was referred to by the authors with no mention of a followup work.[78]

2.7. Zinc

2.7.1. Introduction

^{67}Zn Mössbauer spectroscopy offers extremely high resolution for the determination of small changes in γ-ray energy.[130−137] The very high sensitivity has proved useful for precision measurements of hyperfine interactions and in gravitational red-shift experiments.

2.7.2. Principles and Properties of ^{67}Zn Mössbauer Spectroscopy

The 93.31-keV Mössbauer spectroscopic state in ^{67}Zn can be populated from ^{67}Ga, $T_{1/2}$ = 78.26 h, and

from ^{67}Cu, $T_{1/2} = 61.9$ h. ^{67}Zn Mössbauer spectroscopy experiments usually have to be carried out at 4.2 K, particularly because the high gamma energy leads to a low recoil-free fraction. However, in favorable cases (hard lattices) the temperature can be extended to ~100 K. Since the natural abundance of ^{67}Zn is only 4.1%, absorbers have to be prepared from ^{67}Zn-enriched material. This makes ^{67}Zn Mössbauer spectroscopic experiments expensive. In the majority of ^{67}Zn experiments, the decay from ^{67}Ga is utilized. The advantage gained is that the ^{67}Ga activity is produced "in situ" in the appropriate source matrix, which contains Cu or Zn by the use of nuclear reactions in a cyclotron. Cu metal disks and single crystals of ZnO have proved to be successful source matrices.

2.7.3. Chemical Properties

From the point of view of phosphor chemists, Zn is an activator, as in ZnO:Zn for example, and is an important host lattice in the ZnS:M phosphors.

Many simple Zn compounds have been studied, including both cubic and hexagonal ZnS. The Mössbauer spectroscopic parameters of the latter two are very similar.[138] This agrees with the facts that the ccp and hcp structures differ only by stacking sequences, and the nearest-neighbor Zn−S bond lengths are nearly equal in the structures.[139] The phosphor chemist probably has much to gain from studying Zn host lattices for subtle differences. However, some phosphors, such as ZnO:Ga, may yield interesting data. In the latter case, this ultrafast phosphor may be studied by conventional methods to study the Zn site, but also the role of the Ga could be studied by emission or source experiments, where ^{67}Ga is put into the phosphor so that the ^{67}Zn Mössbauer spectroscopic nuclei are formed at the Ga lattice sites after the decay of ^{67}Ga. Similarly studies on ZnS:Cu phosphors could be carried out by emission or source experiments where the 93.31 keV level is excited from ^{67}Cu to make sure that the ^{67}Zn Mössbauer spectroscopic nuclei are formed on the Cu lattice sites after decay of ^{67}Cu. Experiments similar to the last two discussed have been carried out to study high T_c superconductors (the Cu sites in $YBa_2Cu_3O_7$ and $YBa_2Cu_3O_6$).[140,141]

2.8. Gadolinium

2.8.1. Introduction

The Mössbauer effect has been found to occur in six different isotopes of Gd: ^{154}Gd, ^{155}Gd, ^{156}Gd, ^{157}Gd, ^{158}Gd, and ^{160}Gd. For a variety of reasons, such as difficulty in preparing good sources or resolution problems, only ^{155}Gd has seen extensive use. It was first observed in 1962.[142]

2.8.2. Principles and Properties of ^{155}Gd Mössbauer Spectroscopy

^{155}Gd has three transitions to low-energy excited states, but the best properties arise from the 86.5-keV gamma rays. The natural abundance of ^{155}Gd is 14.8%. The parent isotope is ^{155}Eu, and the source half-life is 4.96 years. The best sources are either a dilute solution of ^{155}Eu diffused into Pd[143] or the compound $^{154}SmPd_3$ (once irradiated by neutrons to include $^{155}EuPd_3$). The latter source contains ^{156}Eu, which has a half-life of 15 days and can also be used for ^{156}Gd Mössbauer spectroscopy.

For ^{155}Gd Mössbauer spectroscopy, it is usual to prepare absorbers with natural Gd. It is only necessary to use enriched ^{155}Gd for materials with low Gd concentrations, particularly where other heavy elements are present. Due to the high-energy elements of the gamma rays, it is advisable to optimize the absorber thickness.[144]

2.8.3. Chemical Properties

A number of early reviews[52,145,146] of Gd Mössbauer spectroscopy in works on rare-earth elements Mössbauer spectroscopy give the parameters for a range of compounds which are of interest to the phosphor chemist. Much work to date has been devoted to magnetic materials, but many of the oxide lattices studied are of interest to the phosphor chemist. Such lattices include $GdAlO_3$,[147,148] $GdVO_4$,[149] $Gd_2M_2O_7$ (M = Sn, Ti, Ru, Ir),[150−155] Gd_2O_3,[153] and Gd_2S_3.[153]

The interest in high-temperature superconductors in the late 1980s sparked a flurry of papers on ^{155}Gd Mössbauer spectroscopy in these materials. Such investigations by Mössbauer spectroscopy are classified on the basis of the sites of the probe nuclei in the cuprates:

(i) Mössbauer spectroscopy of probe rare-earth element nuclei in sites which are normally occupied by rare-earth element atoms.

(ii) Mössbauer spectroscopy of nuclei of atoms which are substituted on Cu sites; these are mainly ^{57}Fe, ^{119}Sn, and ^{67}Zn (see section on ^{67}Zn).

Mössbauer spectroscopy using ^{155}Gd is confined to the first class and is mentioned here simply to show that similar studies could easily be applied to Gd-containing phosphors (using enriched ^{155}Gd if the amount of Gd present in the phosphor is low). $GdBa_2Cu_3O_7$ has been studied by many groups;[156−165] $(Gd_{1-x}Pr_x)Ba_2Cu_3O_7$[166] and $GdBa_2Cu_4O_8$ have also received attention.[167] Studies on $Bi_{4-x}Gd_xSr_3Ca_3Cu_4O_z$ (where $x = 0.3$ or 0.5) and $Bi_2Sr_2Ca_{1-y}Gd_yCu_2O_z$ (where $y = 0.25$ or 0.5) using ^{155}Gd Mössbauer spectroscopy have been interpreted to indicate that the Gd has a strong preference to occupy the Ca sites.[168] This latter study illustrates that, even at relatively low Gd concentrations, useful information can come out of such studies.

The importance of Gd_2O_3 as a host lattice for phosphors, and the fact that Gd is often added to yttrium oxide lattices by phosphor chemists, make ^{155}Gd Mössbauer spectroscopy potentially a very important technique for phosphor research.

2.9. Other Rare-Earth Elements

In addition to the above elements, four other elements that are of interest to the phosphor chemist can be studied using Mössbauer spectroscopy: dysprosium, erbium, thulium, and ytterbium. However, little Mössbauer spectroscopy has been carried out on these elements, and to our knowledge there have been no studies specifically aimed at phosphor ma-

terials for phosphor research. We will therefore be very brief in our description of these elements.

2.9.1. Dysprosium

Of the four possible isotopes that have Mössbauer spectroscopic resonances, ^{160}Dy, ^{161}Dy,^{162}Dy, and ^{164}Dy, only^{161}Dy has a relatively low gamma energy (25.65 keV), and it was extensively studied in the early years of Mössbauer spectroscopy. ^{161}Dy has an isotopic abundance of 18.88%, and the parent source isotope ^{161}Gd has a 6.9-day half-life. A number of metal oxide lattices[169−171] have had their Mössbauer spectroscopic parameters reported, including Dy_2O_3.[171]

2.9.2. Erbium

Five Er isotopes have Mössbauer spectroscopic resonances: ^{164}Er, ^{166}Er, ^{167}Er, ^{168}Er, and ^{170}Er. All of these have large gamma energies.^{166}Er has an isotopic abundance of 33.41%, and the parent source isotope ^{166}Ho has a half-life of about 1200 years. Some intermetallic compounds[172−175] have been studied using this Mössbauer spectroscopic isotope.

2.9.3. Thulium

The 8.40-keV gamma ray energy of ^{169}Tb is populated from^{169}Er with high efficiency, and this low energy is compatible with a good Mössbauer resonance. However, a number of drawbacks reduce the resonance absorption to around the 1% level. Some work has been reported on the Tm_2O_3 lattice which is of interest to phosphor chemists.[176,177]

A more recent study using ^{169}Er to give ^{169}Tb in situ to observe vacancy trapping after implantation into aluminum at low temperature (5 K) has been reported.[178] Due to the presence of a local 4f moment that is orientated by the neighboring atoms, large quadrupole interactions were found for non-cubic electronic environments. A quadrupole doublet that was observed in the 100−300 K region was ascribed to vacancy association.

2.9.4. Ytterbium

There are five possible isotopes in Yb that have Mössbauer spectroscopic resonances: ^{170}Yb, ^{171}Yb, ^{172}Yb, ^{174}Yb, and ^{176}Yb. All have gamma ray energies of about 70−80 keV, and of these both ^{170}Yb and ^{171}Yb have been studied. High-pressure Mössbauer spectroscopic studies in a diamond anvil cell have been carried out on Yb_2O_3 using the 84.3-keV transition in ^{170}Yb enriched to 70%.[179] The sample used was cubic Yb_2O_3. The isomer shift was insensitive to pressure changes. At higher pressures (about 14 GPa) the cubic to monoclinic transition took place. This was confirmed by X-ray diffraction data at room temperature after decompression when the monoclinic structure remained. This type of work, though carried out for other reasons, is extremely important for the study of phosphors.

3. Raman Spectroscopy

3.1. Historical Background

The Raman effect takes its name from C. V. Raman, who discovered the effect in 1928.[180,181] It is an inelastic light-scattering phenomenon that is analogous to the Compton effect which is observed for X-rays.

There are many reviews of Raman spectroscopy of various types of compounds in the solid state, for example biomaterials, pigments, minerals, semiconductors, and low-temperature superconductors.[182−190] However, to our knowledge, there has not been a review of the Raman spectroscopy of phosphors.

Raman spectroscopy is a valuable tool for the characterization of phosphors, as it is sensitive to both the composition and the structure of the lattices. As will be shown herein, it can provide information not only on the structure of the hosts of doped phosphor-type materials but also on the site symmetries of the dopants.

The majority of Raman spectroscopic studies of the solid state are concerned with the vibrational properties of the solids, and these will be dealt with in the next section. The vibrational Raman spectrum of a phosphor can be collected in a matter of minutes with modern Raman instrumentation, and, as will be seen, it readily enables the phase of the phosphor lattice to be identified. Moreover, the use of a Raman microscope enables particles of micrometer dimensions to be analyzed, and this has proved invaluable for assessing the homogeneity of phosphor samples.

A relatively smaller number of solid-state studies have concentrated on the electronic Raman effect, and these will be discussed after the section on vibrational Raman spectroscopy. The usefulness of electronic Raman spectroscopy stems from the fact that intramanifold transitions take place between levels of the same parity; thus, they are Raman active but electric dipole forbidden. Consequently, electronic Raman spectroscopy enables low-lying levels to be located; these levels are difficult to characterize by other means.

3.2. Vibrational Raman Spectroscopy

3.2.1. Introduction

The vibrational Raman spectra of phosphors yield information about the crystallographic phases, the lattice phonon energies, and the site symmetries of activators, all of which are important parameters, as these factors critically affect the efficiencies of the luminescence.

In this section of the review, the Raman spectra of phosphors will be discussed according to the classification of the lattice type, namely binary, ternary, and miscellaneous. Each of these will be covered in a separate section.

3.2.2. Oxides MO

ZnO. Films of ZnO have been deposited at room temperature, 230 °C, and 430 °C by a filtered cathodic vacuum arc technique, and the films deposited at room temperature were found to be amorphous whereas the films grown at the higher temperatures were polycrystalline.[191] Evidence for the polycrystallinity came from the Raman spectra, which showed two peaks at 436 and 556 cm^{-1} that are due to the E_2 and E_1(LO) modes of ZnO in the

wurtzite phase, respectively.[192] Zinc oxide is often a nonstoichiometric compound which can have an excess of zinc in the lattice to varying degrees, depending on the method of preparation. It has been proposed that the impurity states introduced by excess zinc in the film stimulate the onset of resonance Raman enhancement at longer wavelengths (e.g., 488 nm) than seen in stoichiometric ZnO.[192] Thus, it was possible to use the intensity of the 556 cm^{-1} band to assess the extent of oxygen deficiency in the ZnO films.[191] By this means, the films grown at room temperature were found to be significantly oxygen deficient, whereas the oxygen deficiency was reduced in the polycrystalline films which were grown at the higher temperatures. The polycrystalline films of ZnO showed strong, near-band-edge room-temperature photoluminescence emission at approximately 380 nm, which was also attributed to the reduced oxygen vacancies as determined by Raman spectroscopy; the green emission peak around 520 nm, which originates from defects in the films, was strongly quenched.[191]

It is noteworthy that phonon frequency shifts from those observed in single crystals of ZnO can be measured by Raman spectroscopy and used to estimate the residual film stress and how it changes with deposition method.[192]

3.2.3. Oxides M_2O_3

Eu^{3+} and Tb^{3+} doped into M_2O_3 (where M is Y^{3+} or a trivalent rare-earth ion) are an important class of phosphors as well as being precursors for other luminescent materials;[193,194] these phosphors will be dealt with later on in the section on rare-earth element-doped Y_2O_3.

Rare-earth sesquioxides are refractory materials which all melt above 2350 °C and are known to exist in three different structural modifications, namely the A, B, and C types.[195] The A type is a hexagonal structure belonging to the space group $P3m$ (D_{3d}^3), the B type is monoclinic belonging to space group $C2/m$ (C_{2h}^3), and the C type is the cubic structure of the mineral bixbyite, $(Fe,Mn)_2O_3$, belonging to space group $Ia3$ (T_h^7). The cation is seven-coordinate in the A-type structure, having a coordination sphere consisting of an octahedral group of O^{2-} ions with an additional O^{2-} ion above one of the octahedron faces.[195] The B-type lattice apparently has three crystallographically nonequivalent cations. All three cation sites have seven-fold coordination: two have monocapped trigonal prism geometries, and the third is described as a distorted octahedron with the seventh O^{2-} ion at a long distance.[196−198]

In the C-type bixybite structure, the cations occupy two crystallographically inequivalent six-coordinate sites: one of these sites, having C_2 symmetry, has the cation at the center of a distorted cube with two O^{2-} ion vacancies on one face diagonal, and the other site, having S_6 symmetry, has the cation at the center of a distorted cube with two O^{2-} ion vacancies on one body diagonal (see Figure 1). The ratio of C_2:S_6 sites is 3:1.

The structures of the various rare-earth sesquioxides depend on the ionic radii and electronegativities of the rare-earth cations; thus, under ambient conditions the trivalent rare-earth cations of large ionic radii (La, Ce, Pr, and Nd) form sesquioxides having the A-type structure. The trivalent cations of Sm, Eu, and Gd have intermediate ionic radii as a consequence of the lanthanide contraction, and these form stable sesquioxides having the B-type structure under normal conditions, whereas the trivalent cations of Tb, Dy, Ho, Er, Tm, Yb, and Lu have smaller ionic radii and give stable sesquioxides having the C-type structure. Yttrium, which has a trivalent ionic radius and electronegativity similar to those of the rare-earth elements, especially holmium and erbium, also forms a sesquioxide having the C-type structure.[199−202] However, the phases of these sesquioxides are dependent on temperature[203,204] and pressure.[196,205−207] For example, the C-type (cubic) Sm and Gd sesquioxides have been reported to transform under pressure to the A-type (hexagonal) structure and then to the B-type (monoclinic) structure upon release of pressure,[208,209] and C-type Eu_2O_3 is apparently believed to behave similarly under pressure.[210]

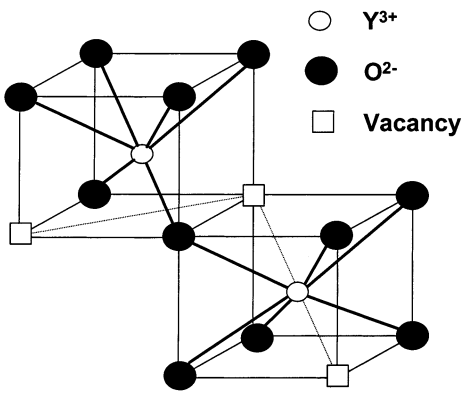

Figure 1. C_2 and S_6 sites of the Y^{3+} cation in cubic Y_2O_3. These sites have vacancies on a face diagonal and a body diagonal, respectively.

Table 8. Raman-Active Modes of Cubic Y_2O_3

Schaak and Köningstein[213]	White and Keramidas[215]	Gouteron et al.[214]	Repelin et al.[217]
597 F_g	603	592 F_g	591 $F_g + A_g$
	576	567 E_g	564 $F_g + E_g$
			526 F_g
473 F_g	480	468 F_g	469 $F_g + A_g$
434 F_g	440	430 F_g	429 $F_g + E_g$
		402 F_g	399 F_g
381 $F_g + A_g$	389	383 E_g	376 $F_g + A_g$
		379 F_g	
333 E_g	337	330 F_g	329 $F_g + E_g$
320 $F_g + E_g$	325	318 F_g	318 F_g
		194 E_g	193 $F_g + E_g$
		182 F_g	179 F_g
164 $F_g + A_g$	162	161 $F_g + A_g$	161 $F_g + A_g$
133 F_g		130 F_g	129 F_g
			116 F_g

Y_2O_3. The cubic form is a common phosphor lattice. Cubic Y_2O_3 is predicted to have 22 first-order Raman-active modes,[211−217] and those that have been observed are listed in Table 8, along with their symmetry types. Furthermore, a Raman spectroscopic study of undoped Y_2O_3 as a function of pressure gave evidence for two phase transitions when the pressure was increased to 22 GPa.[211] These were identified

Table 9. Unit Cell Parameters, Raman Wavenumbers of the Intense Phonon Band in the 370 cm^{-1} Region, and Ionic Radii of the Dopant in Cubic Y_2O_3:Ln, 10 mol % (Taken from Ref 219)

sample	cell parameter (Å)	Raman shift (cm^{-1})	rare-earth ionic radius (Å)
Y_2O_3:Nd	10.681 ± 0.0025	370	0.980
Y_2O_3:Eu	10.659 ± 0.0022	371	0.947
Y_2O_3:Gd	10.647 ± 0.0030	374	0.938
Y_2O_3:Tb	10.635 ± 0.0036	373	0.923
Y_2O_3:Ho	10.630 ± 0.0044		0.901
Y_2O_3:Er	10.620 ± 0.0008		0.890
pure Y_2O_3	10.616 ± 0.0033	377	

from the Raman spectra as C → B and B → A phase transitions; the former was detected at a pressure of 12 GPa and is reported to be first order and irreversible, whereas the latter was detected at 19 GPa and is reported to be first order and reversible (the pressure effects will be dealt with in more detail at the end of this section). When there is temperature-dependent polymorphism, the A, B, and C structures are typically those of the high-, medium-, and low-temperature forms, respectively.[195]

We have recently used Raman spectroscopy to determine the temperature at which Y_2O_3:Eu^{3+} phosphor samples crystallize from hydroxycarbonate precursors.[218] The intensity of the cubic Y_2O_3 band at 377 cm^{-1} is correlated to the degree of crystallinity of the Y_2O_3:Eu^{3+} phosphor powders. It should be noted that the exact wavenumber location of this band does apparently vary depending on rare-earth cation dopants (see Table 9).[219]

Y_2O_3:Eu^{3+} has been used as a red photoluminescent phosphor in lamps and cathodoluminescent phosphor in color television. In this lattice the Eu^{3+} ions substitute the Y^{3+} ions which occupy C_2 and S_6 sites in a ratio of 3:1.[220−222] An important additional benefit of Raman spectrometers for phosphor chemists is that they can collect the laser-excited luminescence spectra of such phosphors. The emission spectrum obtained in this way from Eu^{3+} in C-type M_2O_3 (where M is Y^{3+} or a trivalent rare-earth ion) under visible or near-ultraviolet excitation occurs mainly from the $^5D_0$ level, although some weak emission lines occur at wavelengths shorter than the $^5D_0 \rightarrow {}^7F_0$ line at ca. 580 nm due to $^5D_1 \rightarrow {}^7F_J$ transitions.[223,224] The weakness of these emission lines is due to the proximity of the $^5D_1$ (∼19 200 cm^{-1}) and $^5D_0$ (∼17 200 cm^{-1}) levels. Raman spectroscopic data suggest that the host lattices have phonon energies as high as 600−700 cm^{-1} (see below), so that the separation of around 2000 cm^{-1} can be bridged by three phonons, resulting in efficient multiphonon de-excitation. Efficient multiphonon de-excitation can also occur from the $^5D_2$ level (∼21 500 cm^{-1}), which is approximately 2300 cm^{-1} higher in energy than the $^5D_1$ level. Thus, upconversion emission was found to be a relatively inefficient process when Y_2O_3:Eu^{3+} was excited by 632.8 nm laser light, compared to the cases of Y_2O_3:Er^{3+}, Y_2O_3:Tm^{3+}, and Y_2O_3:Ho^{3+}.[221,222,225,226]

In commercial Y_2O_3:Eu^{3+} phosphors, the $^5D_0 \rightarrow {}^7F_0$ transition of Eu^{3+} occupying C_2 sites of Y_2O_3 is located at 580.8 nm, and a weak, narrow excitation peak at 578.0 nm has been identified for the same transition of Eu^{3+} in S_6 sites.[213] The structure in the excitation spectra at shorter wavelengths was identified as the vibronic overtones of the $^5D_0 \rightarrow {}^7F_0$ transition. This was supported by a satisfactory correlation of the phonon maxima derived from the C_2-type vibronic spectra and the reported Raman and infrared data.[212,213] However, a correlation was less evident when contrasting the vibronic spectra for the S_6 sites with the Raman and infrared data. For these commercial phosphors, having an Eu^{3+} concentration of ca. 4.7 mol %, efficient energy transfer occurs between the S_6 and C_2 sites for Eu^{3+} in the $^5D_0$ level. As the $^5D_0$ level in the S_6 site is 87 cm^{-1} higher than the same level in the C_2 site, the efficient energy transfer from S_6 to C_2 sites presumably occurs by simultaneous creation of a phonon.[213] This efficient energy transfer is necessary for the high emission efficiency of the Y_2O_3:Eu^{3+} phosphor, as the $^5D_0 \rightarrow {}^7F_2$ transition which gives rise to the red 611 nm emission is electric dipole allowed for Eu^{3+} in C_2 sites but forbidden for Eu^{3+} in S_6 sites.

It has recently been reported that, when nanocrystalline material is condensed from the gas phase, the B-type monoclinic form of Y_2O_3:Eu^{3+} can be prepared,[227−230] and the formation in the monoclinic phase has been attributed to the Gibbs−Thompson effect.[231] This effect refers to the stabilization of the high-temperature phase due to the higher surface area to bulk volume ratio found in these nanoparticles. The cubic phase does form, however, as the particle size decreases to 7 nm.[227] There is currently much interest in nanocrystals which can form in new phases because they can exhibit enhanced electronic and optical properties. The B-type phase of Y_2O_3 was identified[211] by comparing its Raman spectrum to those of B-type Sm_2O_3, Eu_2O_3, and Gd_2O_3.[232,233] Furthermore, a good linear correlation was observed between the highest frequencies of the vibrational modes of B-type Y_2O_3 and pressure, and this allowed the values of the *c*/*a* ratio of the monoclinic unit cell to be deduced over a range of pressures up to 18 GPa.[211] The values of the *c*/*a* ratio are related to the compactness of the unit cell, and these were in good agreement with those given by others.[207,234,235]

Four intense bands were observed in the Raman spectrum of Y_2O_3 under a pressure of 22 GPa. Two bands at 577 and 537 cm^{-1} can be assigned to stretching modes of A-type Y_2O_3, and the other two bands at 320 and 174 cm^{-1} can be assigned to bending modes by analogy with the bands observed in the Raman spectrum of A-type Sm_2O_3.[211] It has been noted that the Y−O bonds are very similar in length in the Y_2O_3 A- and B-type structures, and the stretching vibrations have similar frequencies in the two structures.[211]

La_2O_3 and Nd_2O_3. Single-crystal Raman spectroscopic measurements have been obtained from these A-type (hexagonal) oxides.[236] The Raman spectra were found to be in exact agreement with predictions from factor group analysis that the oxides, which belong to space group $P3m$ (D^3_{3d}), should have $2A_{1g} + 2E_g$ Raman-active modes. Complementary infrared spectra of Nd_2O_3 were also in agreement with the

factor group analysis which predicts that the oxides should have $2A_{2u} + 2E_u$ infrared-active modes.

Sm_2O_3. Raman-active phonon spectra of both B (monoclinic) and C (cubic) structures of Sm_2O_3 were observed[237] and confirmed previous results.[215,232] Of the 22 Raman-active modes predicted by group theory for the C-type structure, 19 were observed, whereas of the 21 Raman-active modes predicted by group theory for the B-type structure, 18 were observed.[237] A transition from the C-type structure to the B-type occurs at a temperature of ca. 850 °C, as evidenced by the Raman spectrum. A Raman-active crystal field excitation was also observed in the C-type structure around 1004 cm^{-1}, and this was associated with the S_6 site symmetry.[237]

The A-type structure of rare-earth sesquioxides has one formula unit per unit cell, and consequently the Raman spectrum exhibits only four bands. This is nicely illustrated by the spectrum of Sm_2O_3, which shows two bands due to stretching modes at 455 and 444 cm^{-1} and two bands due to bending modes at 188 and 105 cm^{-1}.[232]

Gd_2O_3. Gadolinium oxide and europium-doped gadolinium oxide waveguiding thin films have been prepared by sol−gel methods,[238,239] and waveguide Raman spectroscopy (WRS) has been conducted on annealed films of Gd_2O_3:Eu^{3+},which have scintillation properties.[239] WRS is a sensitive, nondestructive technique for the analysis of such films below 900 °C, but above this temperature the films are reported to lose their waveguiding properties. To perform WRS, a focused laser beam must be coupled into the thin film being used as the waveguide. The most convenient way of doing this is to use a coupling prism.[240,241] The prism is clamped against the film using adjustable thumbscrews, allowing an evanescent field to pass through the thin coupling air gap and launch light into the waveguide. The prism is mounted on a translation stage at the center of a goniometer, which enables the coupling angle to be selected precisely so that a guided light mode can be launched in the film. This light excites Raman scattering within the film, and the scattered light can then be collected normal to the propagation direction of the light beam within the planar waveguide. This allows high signal-to-noise Raman spectra of thin films to be collected.

The Raman spectra collected in this way indicate that the films transform from the amorphous phase into the crystallized phase at 600 °C. The Raman spectrum of Gd_2O_3 in the amorphous phase is manifested by two weak broad bands around 90 and 350 cm^{-1},[238,239] whereas the Raman spectrum of C-type Gd_2O_3 exhibits six bands at 93, 117, 313, 359, 442, and 565 cm^{-1}.[239]

Lu_2O_3. Raman spectra of Lu_2O_3:Er^{3+} have been used to explain some interesting emission phenomena associated with this material.[242] The sesquioxide Lu_2O_3, like Y_2O_3, crystallizes in a cubic structure belonging to the *Ia*3 space group, and Er^{3+} ions substitute for Lu^{3+} ions randomly on C_2 and S_6 sites, which are present in the ratio of 3:1. It has recently been reported that, under identical conditions, nanocrystalline Lu_2O_3:Er^{3+} shows upconversion intensities approximately 100 times greater than Y_2O_3:Er^{3+} under 804-nm light excitation.[242] A possible explanation for the enhanced emission properties of Lu_2O_3:Er^{3+} is that an intensity-borrowing mechanism operates by the mixing of 4f and 5d orbitals of the Lu^{3+} ion via the lattice valence band levels.[243] A comparison of the upconversion luminescence of bulk Lu_2O_3:Er^{3+} with that of the nanocrystalline material showed that the former was significantly more intense.[242] It was suggested that the reason for this is that the latter material has carbonate and hydroxyl ions adsorbed on the surfaces of its nanocrystals and these make available vibrational quanta of ca. 1500 and 3300 cm^{-1}, respectively, for multiphonon relaxation. The Raman spectra of commercial and nanocrystalline Lu_2O_3 were presented[242] to show that the maximum phonon energy of lutetia is about 620 cm^{-1}, which is considerably lower than the vibrational quanta available from the carbonate and hydroxyl ions.

Table 10. Raman Wavenumbers and Assignments for Cubic Lu_2O_3 and Y_2O_3 (Taken from Ref 244)

	observed wavenumbers (cm^{-1})	
assignment	Y_2O_3	Lu_2O_3
T_g	132.8	98
$T_g + A_g$	164	120
	195.7	191
$T_g + A_g$	320.5	289
E_g	333.5	348
$T_g + A_g$	380.9	393
T_g	472.8	499
T_g	597	614

Raman spectra of a single crystal of C-type Lu_2O_3 were reported for the first time by Laversenne et al.,[244] and the Raman frequencies and assignments were compared with those of C-type Y_2O_3 (see Table 10). As can be seen from Table 10, there is good agreement between the frequencies of the respective vibrational modes.

Lu_2O_3 is currently used as a host material for scintillator phosphors.

3.2.4. Oxides AB_xO_4

YVO_4. Raman spectroscopy has helped our understanding of many of the properties of rare-earth element-doped YVO_4 lattices. This lattice doped with Eu^{3+} was the first red phosphor used for color television (in the early 1960s). The first-order Raman spectrum of the yttrium vanadate lattice was reported in detail in 1967.[245] Nine of the 12 Raman-active modes were observed, and symmetry assignments were made.

The Raman spectra of YVO_4 crystals doped with 1% Nd^{3+} showed bands at essentially the same wavenumbers as undoped YVO_4, viz. 159, 165, 261, 379, 490, 816, 839, and 892 cm^{-1}.[246] In another study of YVO_4:Nd^{3+} crystals, two broad Raman bands in the 300−400 and 700−1000 cm^{-1} regions gave evidence for the formation of an impurity phase in addition to YVO_4.[247] The investigation of these materials was motivated by their laser and luminescence applications.

In the case of Czochralski-grown undoped YVO_4 crystals, a number of Raman bands were observed above 1000 cm^{-1} which were attributed to oxygen deficiency in VO_4 units, resulting in a distortion of VO_4 tetrahedra.[248]

$ZnGa_2O_4$. The spinel, $ZnGa_2O_4$, has an emission which peaks around 390 nm and decays with a short lifetime of around 0.6 ns; for this reason, it has been considered as a scintillator for fast detection systems.[249] When this lattice is doped with either Mn^{2+} or Si^{4+}, promising phosphor materials can be prepared. The Mn-doped $ZnGa_2O_4$ phosphor, $ZnGa_2O_4$:Mn, has been considered as one of the leading candidates as a green-emitting field emission display (FED) phosphor because it has moderate electrical conductivity and good chemical stability.[250] Unfortunately, the oxidation state of the manganese activator was erroneously given as 4+ in that paper.[250] The Si-doped $ZnGa_2O_4$ phosphor, $ZnGa_2O_4$:Si^{4+}, has also been reported for potential applications in FED and plasma display panel (PDP) devices.[250]

The spinel has eight formula units per unit cell and belongs to the space group O_h^7 ($Fd3m$). A factor group analysis shows that it has $\Gamma = A_{1g} + E_g + T_{1g} + 3T_{2g} + 2A_{2u} + 2E_u + 5T_{1u} + 2T_{2u}$ fundamental modes, of which the infrared-active modes are $4T_{1u}$ and the Raman-active modes are $A_{1g} + E_g + 3T_{2g}$. Raman bands at 464 and 609 cm^{-1} have been previously assigned to T_{2g} and A_{1g} modes, respectively.[251] The first-order Raman-active modes in a normal spinel, AB_2O_4, are independent of the motions of B atoms. Thus, the Raman-active modes in $ZnGa_2O_4$ depend only on the motions of Zn^{2+} in tetrahredral sites and O^{2-} ions, whereas there is no contribution from the Ga^{3+} ions in octahedral sites. Raman spectra of $ZnGa_2O_4$:Si^{4+} phosphors exhibited a new band at 540 cm^{-1};[250] consequently, it could be inferred that the Si^{4+} ions substitute the Zn^{2+} ions in tetrahedral sites. The Raman spectra showed that the solid solubility limit of Si in $ZnGa_2O_4$ was 0.05 mole fraction, and this was consistent with the results from XRD measurements. The effect of doping Si^{4+} into the $ZnGa_2O_4$ phosphor was to enhance the PL intensity by a factor of 3 and to shift the emission peak to longer wavelength.[250]

3.2.5. Metal Sulfides (MS)

ZnS. ZnS is an important host lattice for green and blue cathode ray tube (CRT) television phosphors as well as for electroluminescent and long afterglow applications. Near-infrared Raman spectroscopy has been used to characterize green-emitting ZnS:Cu,Al materials.[252] Excitation of wavelength equal to 752.5 nm was employed so that the Raman spectra were free from the strong visible luminescence which occurs from these phosphor materials. A strong Raman band at 350 cm^{-1} due to the LO mode and additional weak features around ~220 cm^{-1}, probably arising from a two-phonon process, indicate that the phosphor had a cubic zinc blende lattice. The Raman spectra of ZnS:Cu,Al samples with different luminescence intensities were compared, and it was found that crystal imperfections can lead to a reduction of luminescence properties. Moreover, there appeared to be a close relationship between the LO mode intensity and the luminescence efficiency. This was interpreted to mean that there was a close relationship between the local structure and the luminescence efficiency. An additional Raman feature appeared at 300 cm^{-1}, along with two broad features at 100−220 and 350−400 cm^{-1}, suggesting that some kind of disordering occurred in the crystal structures of low luminescence samples. The most plausible explanation was that there was a local symmetry breaking due to defect structures associated with intergrowths of hexagonal domains. This was indicated by a Raman band at 300 cm^{-1}, which was attributed to the E_2 mode of ZnS in the hexagonal phase for which the cubic phase has no counterpart. It was emphasized that Raman spectroscopy is sensitive to short-range order (of the order of approximately ≥5 unit cells), unlike XRD, which has a coherence length of ≥20 unit cells,[252] allowing the detection of polymorphic modifications of the phosphor. It was pointed out that an advantage of Raman spectroscopy over XRD is that the polymorphic modifications of nanometer-sized particles can be detected by the former technique, whereas line broadening occurs when using XRD, and that hinders the ability of this latter technique to distinguish between different polymorphic modifications.

Bulk ZnS:Ag,Al is a blue-emitting CRT television phosphor. Nanocrystalline particles of ZnS:Ag,Al have been studied by Raman spectroscopy as well as transmission electron microscopy.[253] The Raman spectra showed that the gas-phase condensation method produced nanoparticles. It is desirable for these CRT phosphors to have small particle sizes in order to increase the resolution and display brightness under low-energy electron beam excitation. The Raman LO phonon band of the ZnS:Ag,Al nanoparticles at ~350 cm^{-1} was shifted by 2.8 cm^{-1} to lower energy from its counterpart in the bulk powder, and the line width became broad. These features were explained by a relaxation of the wave-vector selection rule due to the quantum confinement effect of the LO phonon.[253−255] These features in the Raman spectrum were accompanied by a large blue shift of the interband absorption edge (at ~3.7 eV) relative to that of the bulk crystal, showing that the quantum confinement effect for the charge carriers occurs in the nanoparticulate sample. It was possible to estimate an average particle size of about 3 nm in diameter from the shift of the absorption band edge using a variational calculation of Brus.[256] This dimension agreed reasonably well with those of the lattice plane images in the TEM micrographs.[253]

3.2.6. Metal Oxysulfides (M_2O_2S)

Y_2O_2S. Eu^{3+}-activated Y_2O_2S is an efficient CL phosphor that is still used today as the red phosphor in CRT television sets. Raman spectra of Ln_2O_2S:Eu^{3+} (Ln = Lu, Y, Gd, and La) have been obtained at room temperature in order to obtain information which would help an understanding of the optical properties of rare-earth element-doped Ln_2O_2S lattices.[257] The lattices of the rare-earth oxysulfides and Y_2O_2S

belong to the space group D_{3d}^3, and the primitive unit cell contains one molecule of Ln_2O_2S.[258] The factor group analysis gives $\Gamma = 2A_{1g} + 2E_g + 2A_{2u} + 2E_u$ optical modes, of which $2A_{1g} + 2E_g$ are Raman active and $2A_{2u} + 2E_u$ are external modes. We note in passing that one of the E_u modes was omitted from the reducible representation that was quoted in the original work.[257] The $2A_{1g} + 2E_g$ Raman-active modes belong to the Ln_2O_2 group, which is a parallelogram. These modes give rise to two pairs of Raman bands, one pair occurring in the low-frequency region with the other pair coming at higher frequency. The low-frequency bands were designated as R_1 and R_2 and are due to $A_{1g} + E_g$ modes, as are the higher frequency bands which were designated as R_3 and R_4.

3.3. Electronic Raman Spectroscopy

3.3.1. Introduction

Electronic Raman spectroscopy is a very useful technique for studying transitions between the ground states and low-lying excited levels of lanthanide ions and can provide much information for the elucidation of the emission spectra of rare-earth element-doped phosphors. These transitions cannot be studied by optical absorption spectroscopy, as they are electric dipole forbidden, but they are Raman active because the initial and final levels have the same parity.

The expression for the Raman scattering amplitude is given by the Kramers Heisenberg equation:[259]

$$(\alpha_{\rho\sigma})_{fg} = -\frac{1}{hc}\sum_i \left[\frac{\langle f|\mathbf{e}_s\cdot\mathbf{r}|i\rangle\langle i|\mathbf{e}\cdot\mathbf{r}|g\rangle}{\nu_{gi} - \nu - i\Gamma_i} + \frac{\langle f|\mathbf{e}\cdot\mathbf{r}|i\rangle\langle i|\mathbf{e}_s\cdot\mathbf{r}|g\rangle}{\nu_{gi} + \nu_s - i\Gamma_i}\right] \quad (1)$$

where ρ and σ are the polarizations of the incident and scattered light respectively; ν and ν_s are the frequencies of the incident and scattered light respectively; $|g\rangle$, $|f\rangle$, and $|i\rangle$ are the ground, final, and intermediate states of the ion, respectively; Γ_i is the half-width at half-maximum (HWHM) of the intermediate state $|i\rangle$; and ν_{gi} is the frequency corresponding to the ground to intermediate state energy separation.

The summation in eq 1 extends over all intermediate states of the active ion.

The electronic Raman selection rules have been compiled by Kiel and Porto.[260] The electronic Raman transition $f \leftarrow i$ is governed by the matrix element

$$[\alpha_Q^K]_{fi} = \langle\psi_f^0|\alpha_Q^K|\psi_i^0\rangle \quad (2)$$

where the irreducible spherical tensor components α_Q^K can be obtained from the Cartesian tensor components $\alpha_{\rho\sigma}$ of eq 1 by a unitary transformation

$$\alpha_Q^K = \sum_{\rho,\sigma} U(K,Q,\rho,\sigma)\alpha_{\rho\sigma} \quad (3)$$

and the orbital parts of the eigenfunctions of the lanthanide ions are given by

$$\psi_i^0 = \sum_m a_{im} Y_m^l \quad (4)$$

$$\psi_f^0 = \sum_{m'} a_{fm'} Y_{m'}^{l'} \quad (5)$$

where Y_m^l and $Y_{m'}^{l'}$ are spherical harmonics characterized by the quantum numbers n, L, S, J, and J_z, the crystal field states being linear combinations of J and J_z; the a_{im} and $a_{fm'}$ are coefficients.

Substitution of ψ_i^0 and ψ_f^0 from eqs 4 and 5 into eq 2 gives

$$[\alpha_Q^K]_{fi} = \langle\psi_f^0|\alpha_Q^K|\psi_i^0\rangle = \sum_{m'}\sum_m a_{fm'}a_{im}\langle Y_{m'}^{l'}|\alpha_Q^K|Y_m^l\rangle \quad (6)$$

This matrix element can be expressed, by use of the Wigner−Eckart theorem, as

$$[\alpha_Q^K]_{fi} = \sum_{m'}\sum_m a_{fm'}a_{im}(-1)^{l-m}\begin{pmatrix} l' & K & l \\ -m' & Q & m\end{pmatrix}\langle l'||\alpha_Q^K||l\rangle \quad (7)$$

where $\begin{pmatrix} l' & K & l \\ -m' & Q & m\end{pmatrix}$ are the Wigner 3j coefficients and $\langle l'||\alpha_Q^K||l\rangle$ are reduced matrix elements.

The basis of electronic Raman selection rules is formed by the Wigner 3j coefficients, which are nonzero only if the sum of any two of l, K, and l' is equal to the third member and $-m' + Q + m = 0$. This allows us to find the components of α_Q^K that transform as the direct product $\Gamma(Y_m^l) \otimes \Gamma(Y_{m'}^{l'})$, which is a prerequisite for a Raman process to be allowed.[261] In the case of a lanthanide ion, l is replaced with J and m is replaced with J_z, so that the Wigner 3j coefficient becomes

$$\begin{pmatrix} J' & K & J \\ -J_z' & Q & J_z\end{pmatrix}$$

The case of Eu^{3+} can be considered as an example. For the $^7F_1 \leftarrow {}^7F_0$ transition, $Q = J_z' - J_z$ and $K = J' + J$, so that the components are α_Q^1 (where $Q = -1$, 0, +1). It is interesting that this electronic Raman process is related to an antisymmetric tensor, as this contrasts vibrational Raman processes which are related to symmetric tensors unless resonance conditions are achieved. For the $^7F_2 \leftarrow {}^7F_0$ transition, the irreducible tensor components are α_Q^2 (where $Q = -2, -1, 0, 1, 2$), indicating that this Raman process is allowed and that it is related to a symmetric tensor. In the same way, it can be shown that the $^7F_3 \leftarrow {}^7F_0$ transition as well as transitions from $^7F_0$ to ^7F_J ($J = 4, 5, 6$) are not allowed.[261] Thus, the electronic Raman selection rule is given by $\Delta J \leq 2$. It should be noted here, however, that electronic Raman lines due to the forbidden $^7F_3 \leftarrow {}^7F_0$, $^7F_4 \leftarrow {}^7F_0$, $^7F_5 \leftarrow {}^7F_0$, and $^7F_6 \leftarrow {}^7F_0$ transitions of Eu^{3+} can be observed when a strong crystal field is experienced by the Eu^{3+} ion; this results in mixing of J states by the crystal field.

The following discussion will refer to the energy level diagram of LSJ states of a number of the trivalent lanthanide ions.[262] This so-called Dieke diagram is presented in Figure 2. The states shown in Figure 2 are split by the crystal field, and the

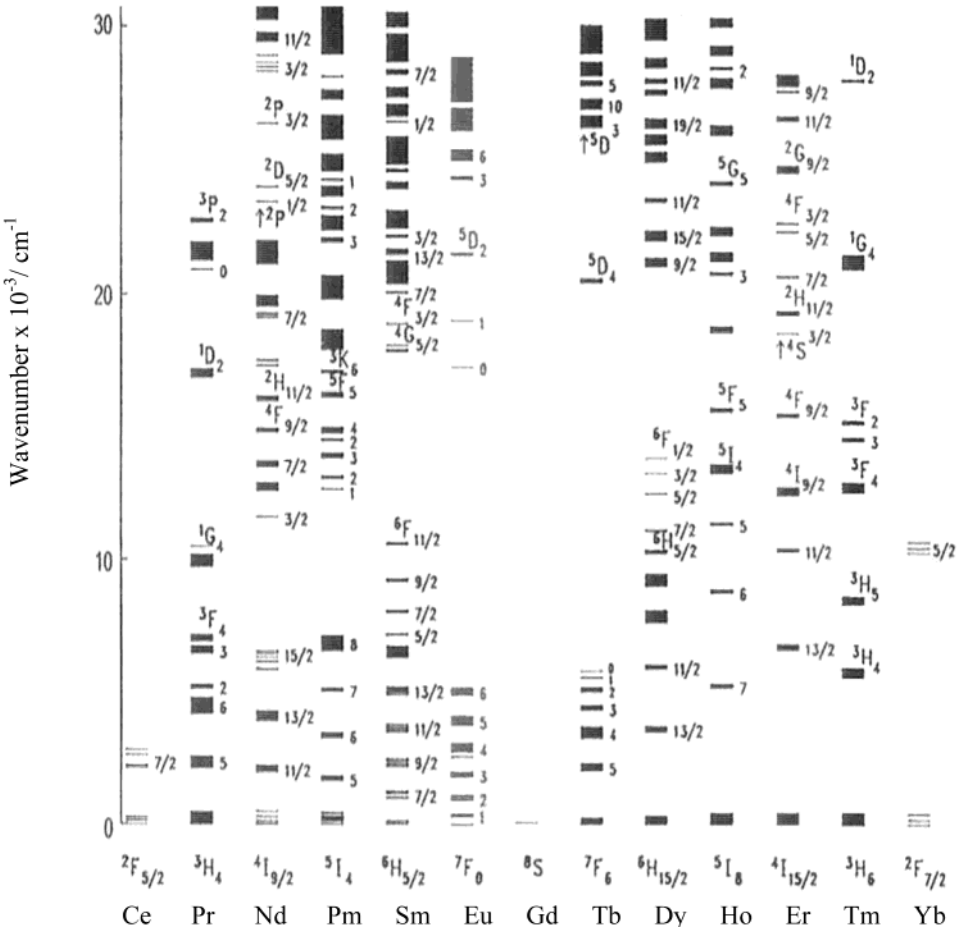

Figure 2. Dieke diagram (adapted from ref 262). This shows the energy levels of the trivalent rare-earth cations.

number of split levels is determined by the crystal field symmetry. It is an interesting feature of the electronic Raman effect that, for ions with an odd number of electrons, all crystal field levels are twofold degenerate, even if the symmetry of the environment is monoclinic. The degeneracy of the Kramers doublets can be removed only in the presence of a magnetic field. Unlike the case of vibrational Raman spectroscopy, there is no factor group splitting, as there is no coupling between ions in the same unit cell.

3.3.2. Phosphors Containing Ce^{3+}

When a sample contains an ion in more than one type of site, such as a rare-earth cation in cubic Y_2O_3, resonant excitation of one of the sites would result in selective enhancement of electronic transitions belonging to that site compared to those of nonresonant sites. For example, electronic Raman transitions of Ce^{3+} in the C_2 and S_6 sites of cubic Y_2O_3 have been selectively enhanced by choosing the wavelength of the laser excitation to coincide with the 4f → 5d absorptions of Ce^{3+} in the C_2 and S_6 sites, respectively.[264] It has been reported that these absorptions are centered on wavelengths of 441 and 516 nm for the C_2 and S_6 sites, respectively, and the electronic transitions for each of these sites have been selectively enhanced by exciting with 457.9 and 514.5 nm laser light. This has enabled the energies of the three Kramers doublets of the $^2F_{5/2}$ ground state to be identified and three of the four Kramer doublets of the $^2F_{7/2}$ excited state for Ce^{3+} cations in S_6 sites (see Table 11).[264] For Ce^{3+} ions in C_2 sites, the energies of two of the three Kramer doublets of the $^2F_{5/2}$ ground state have been identified, along with those of three of the four Kramer doublets in the $^2F_{7/2}$ excited state (see Table 11). These states, which arise from the $4f^1$ ground-state configuration of the Ce^{3+} ion, can be seen in the Dieke diagram of Figure 2.[263] Resonance enhancement factors of 2 orders of mag-

Table 11. Frequency Shift, Linewidth, and Intensity of the Observed Stokes Electronic Raman Transitions of the $4f^1$ Ground Configuration of Ce^{3+} in Y_2O_3 Using 514.5 nm Excitation at a Temperature of 92 K[a]

site	multiplet	frequency shift (cm^{-1})	line width (cm^{-1})	normalized intensity
C_2	$^2F_{5/2}$	666	10.0	0.155
		–	–	–
	$^2F_{7/2}$	2129	3.0	0.375
		2793[b]	8.0[b]	0.225[b]
		–	–	–
		3814	8.0	0.020
S_6	$^2F_{5/2}$	978	6.0	0.609
		1503	15.0	0.268
	$^2F_{7/2}$	2270	3.5	1.215
		2996	8.0	0.915
		3402	8.0	0.155
		–	–	–

[a] Levels not observed by electronic Raman spectroscopy are indicated by dashes. The intensities were normalized using the intensity of the 379 cm^{-1} vibrational mode of Y_2O_3 (taken from ref 264). [b] These values were obtained with 457.9 nm excitation.

nitude in both the C_2 and S_6 sites were observed using 457.9 and 514.5 nm excitation, respectively. Y_2O_3:Ce^{3+} is only weakly fluorescing under short-wavelength ultraviolet excitation.[265] However, a luminescent material containing the same activator, YAG:Ce^{3+}, is a useful yellow light-emitting phosphor when excited in the blue region. This phosphor is presently finding applications in white light-emitting phosphor-coupled LEDs. These consist of a layer of the phosphor on the LED chip, and they generate white light from a combination of the yellow phosphor emission with the complementary blue light emitted by the LED.[266]

3.3.3. Phosphors Containing Eu^{3+}

Early polarized electronic Raman effects were reported for YVO_4:Eu^{3+},[267] which was identified as a commercial red cathodoluminescent phosphor for television sets in the early 1960s, as was previously mentioned in section 3.2.4.[193] In this phosphor the Eu^{3+} cations replace the yttrium ions of the tetragonal YVO_4 lattice and thus occupy sites of D_{2d} symmetry. A line at 404.5 cm^{-1} in the spectrum of a single crystal had a half-width that decreased strongly upon cooling the sample, unlike the vibrational Raman bands of YVO_4, which is typical of the behavior of electronic Raman lines. The polarization properties of this electronic Raman line were similar to those of the 840 cm^{-1} vibrational band of the YVO_4 lattice, indicating that the former has E symmetry, as does the latter. Consequently the 404.5 cm^{-1} electronic Raman line could be assigned to the E component of the low-lying $^7F_1$ state of Eu^{3+}, which is split into B_2 and E components by the crystal field.[267] A weak Raman line at 359.5 cm^{-1} was presumed to be of electronic origin, and incomplete polarization data for this line were in good agreement with an assumed B_2 assignment. Other electronic Raman lines were observed at 970, 995, 1018, and 1067 cm^{-1} which can be assigned to A_1, B_1, B_2, and E crystal field levels of the $^7F_2$ state, respectively.

Although there is a wealth of information about the splittings of energy levels of rare-earth cations in C_2 sites of cubic Y_2O_3, there is a paucity of experimental data for rare-earth cations in S_6 sites. This is because electric dipole transitions are associated with the former sites but not with the latter ones. The experimental data for ions in S_6 sites come mainly from electronic Raman scattering, from relatively few observations of magnetic dipole transitions identified with ions in S_6 sites, and from g values deduced from EPR measurements of rare-earth cations doped into cubic Y_2O_3. Also, because of the weakness of the electronic and magnetic dipole transitions, most of the data on S_6 sites are for the pure R_2O_3 (where R is a rare-earth cation) sesquioxides which have the same cubic structure as Y_2O_3, i.e., only the heavy lanthanide elements (Ho to Lu).

In an early study of Y_2O_3:Eu^{3+}, another red cathodoluminescent phosphor which has been used commercially in television sets, electronic Raman lines were reported in addition to Raman phonon bands.[213] These electronic Raman lines, which were clearly distinguishable from fluorescence lines, appeared at 830, 948, and 1184 cm^{-1}, and they were assigned to the crystal field split components of the $^7F_2$ state of Eu^{3+} ions in S_6 sites. The $J = 2$ state of the free ion splits into $A_g + 2E_g$ crystal field levels in the S_6 site, and it was possible to assign the 830 and 948 cm^{-1} lines to the two E_g levels and the 1184 cm^{-1} line to the A_g level.[213] The $J = 1$ state of the free Eu^{3+} ion splits into E_g and A_g crystal field levels in the S_6 site, which have been reported at 132 and 432 cm^{-1}, respectively.[268,269] Schaak and Koningstein have shown from their calculations of Raman scattering intensities that $\Delta J = 2$ transitions are favored by a factor of 30 in intensity over the $\Delta J = 1$ transitions.[213] The intensities of transitions with $\Delta J > 2$ are expected to be very weak, and, as far as the authors are aware, there are no experimental data on the $^7F_{3,4,5,6}$ manifolds of Eu^{3+} ions in the S_6 sites. Electronic Raman data have been observed for all the $^7F_{0-6}$ manifolds of Eu^{3+} ions in europium−gallium−garnet (EuGaG), however.[270] Electronic Raman lines due to the forbidden $^7F_3 \leftarrow {}^7F_0$, $^7F_4 \leftarrow {}^7F_0$, $^7F_5 \leftarrow {}^7F_0$, and $^7F_6 \leftarrow {}^7F_0$ transitions occur because the strong crystal field experienced by the Eu^{3+} ion results in a mixing of the crystal field terms derived from the different states. These lines are observed in the 1800−2000, 2400−3200, 3700−4000, and 4900−5300 cm^{-1} regions, respectively.[270] It should be mentioned that electronic Raman spectroscopy is limited to bands $< \sim 10\,000$ cm^{-1} on account of the ν^4 dependence of the scattered light intensity and the fact that the incident radiation is normally in the visible or near-ultraviolet region of the electromagnetic spectrum.[271]

Although electronic Raman scattering by Eu^{3+} ions occupying S_6 sites of Y_2O_3 has been observed, there has been no indication of electronic Raman scattering by Eu^{3+} ions occupying the C_2 sites of Y_2O_3, even though the latter are 3 times more abundant than the former.[213] This can be explained by the fact that the Eu^{3+} ions in the S_6 sites which have centers of inversion would be expected to be more Raman active than those in the C_2 sites which lack one.[272]

3.3.4. Phosphors Containing Tb^{3+}

Electronic Raman spectroscopy has been used to investigate the structure of a thin film of YAG:Tb^{3+}, which is a CRT phosphor, grown by liquid-phase epitaxy (LPE).[273] Using 514.5-nm excitation, electronic Raman lines that were reported at 62 and 72 cm^{-1} were assigned to $^7F_6$ intra-manifold transitions, and further electronic Raman lines at 2123, 2135, 2159, 2187, 2336, 2360, and 2390 cm^{-1} were assigned to $^7F_5 \leftarrow {}^7F_6$ transitions.[273] Comparison of the electronic Raman spectrum of the thin film with the electronic Raman spectrum of single crystals of YAG:Tb^{3+} indicated that Tb^{3+} substitutes for Y^{3+} in the thin films in the same way as it does in the single crystals.[270,274−276]

3.3.5. Phosphors Containing Yb^{3+}

Becker et al.[277] studied both the electronic and the vibrational Raman spectra of a single crystal of $YbPO_4$ which are useful for consideration here, even though the Yb^{3+} ion concentration is too high for it to be a phosphor. The authors reported that the E_g

phonon at 310 cm^{-1} has an anomalously large Raman line width of 50 cm^{-1} at room temperature and that this transition is split into several separate transitions that move apart in energy as the temperature is lowered. These observations were interpreted on the basis of electron−phonon coupling.[277]

4. Studies Combining the Use of Mössbauer and Raman Spectroscopies

The two techniques are complementary in many respects, which makes the combination of these two probes a powerful approach. One can easily see evidence from the electronic Raman spectra for the two cation sites, namely C_2 and S_6, in the Y_2O_3:Eu^{3+} phosphor, whereas this is not so easy with Mössbauer spectroscopy due to overlapping signals for the two sites. Also, whereas the vibrational Raman spectrum probes the vibrations of the whole lattice, the Mössbauer spectrum probes the active center (e.g., Eu^{3+} in the Y_2O_3:Eu^{3+} phosphor). On the other hand, the electronic Raman spectrum probes the electronic transitions of the activator ions and provides information about their excited electronic states. The remainder of this section will consider the Mössbauer/Raman probes when used in combination.

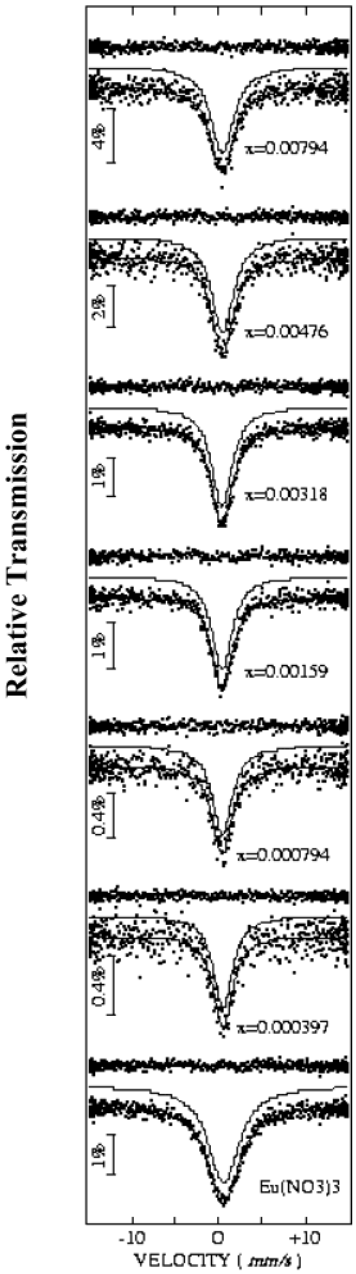

Figure 3. Mössbauer spectra obtained from amorphous samples of $Ti_{1-3x}Eu_{4x}O_2$ doped with different levels of europium (adapted from ref 278).

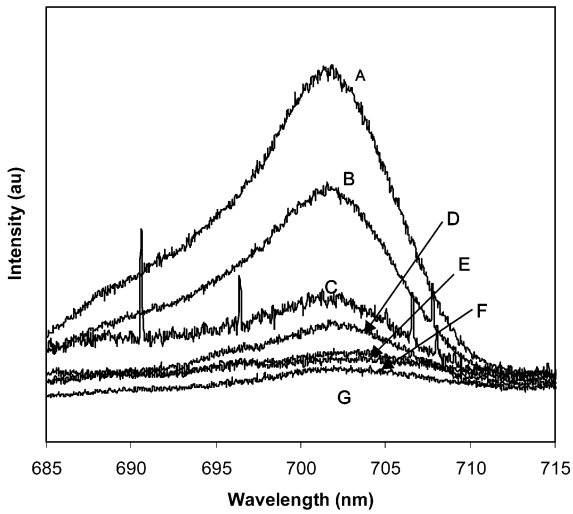

Figure 4. Stokes luminescence spectra obtained from amorphous samples of $Ti_{1-3x}Eu_{4x}O_2$ doped with different levels of europium. (A) $x = 0.00794$, (B) $x = 0.00476$, (C) $x = 0.00318$, (D) $x = 0.00159$, (E) $x = 0.000794$, (F) $x = 0.000397$, and (G) hydrothermal ($x = 0.00318$). Excitation of wavelength equal to 632.8 nm was used in each case (adapted from ref 278).

Recent studies on the effects of Eu^{3+} doping and calcination on the luminescence of titania phosphor materials (of general formulas $Ti_{1-3x}Eu_{4x}O_2$, x varying between 0.000397 and 0.00794) describe the use of Mössbauer spectroscopy to show the presence of multiple sites with different levels of dopant.[278,279] As can be seen from Figure 3, the Mössbauer spectra progressively exhibited broader peaks as the Eu^{3+} concentration increased, indicating that the Eu^{3+} ions were occupying multiple sites within the amorphous material. In addition, Raman studies were used for both structural (phase) investigations and to study the Stokes luminescence spectra excited by the 632.8-nm laser line. It was shown by means of Raman spectroscopy that the crystallization temperature of the titania from the amorphous phase to the anatase phase was raised by addition of Eu^{3+} to the material. The brightness of the emission increased as the Eu^{3+} content was raised to $x = 0.00794$ (see Figure 4). This was the first report of an amorphous inorganic rare-earth element-doped powder phosphor, and it was demonstrated that calcination of the amorphous titania to form rutile or anatase reduces the brightness of the luminescence.[278] The anatase and rutile phases of TiO_2 are easily distinguished from their Raman spectra; both crystallographic forms are strong Raman scatterers, the former giving rise to Raman bands at 398, 514, and 641 cm^{-1} and the latter having bands at 448 and 612 cm^{-1}.[278] A followup work extended the Eu^{3+} concentration to $x = 0.143$. It was shown that the luminescence was due to a TiO_2:Eu^{3+} compound rather than an Eu^{3+}-

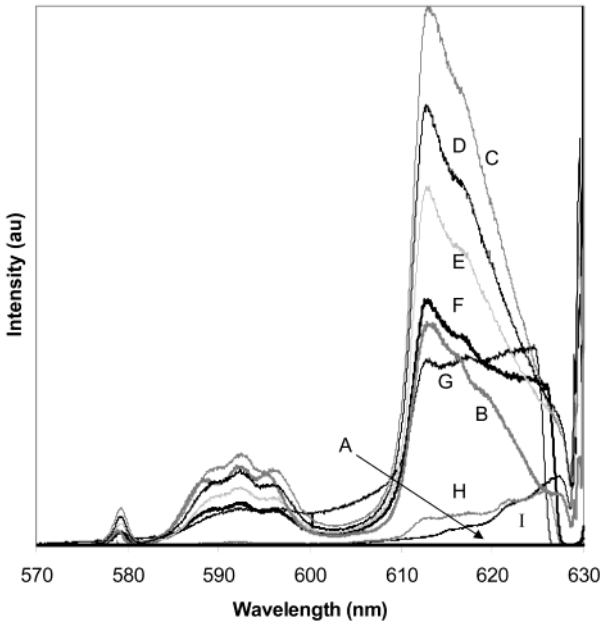

Figure 5. Stokes luminescence spectra obtained from amorphous samples of $Ti_{1-3x}Eu_{4x}O_2$ doped with different levels of europium. (A) Eu_2O_3 starting material, (B) europium nitrate precipitate, (C) $x = 0.143$, (D) $x = 0.0397$, (E) $x = 0.0159$, (F) $x = 0.00794$, (G) $x = 0.00318$, (H) $x = 0.000794$, and (I) TiO_2-only precipitate. Excitation of wavelength equal to 632.8 nm was used in each case (adapted from ref 280).

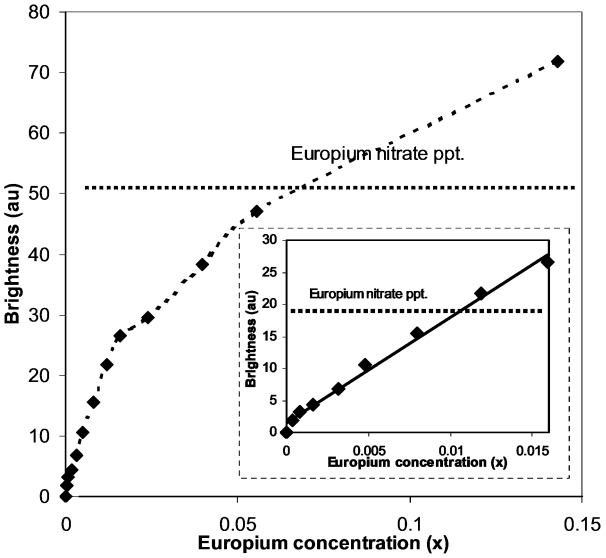

Figure 6. Graph of the intensity of the 613-nm emission band versus europium concentration (x) for amorphous $Ti_{1-3x}Eu_{4x}O_2$ phosphor materials. Excitation of wavelength equal to 366 nm was employed, and the dotted horizontal line indicates the emission intensity obtained from the europium nitrate precipitate over this europium concentration range (adapted from ref 280).

containing precipitate dispersed within a titania precipitate.[280] The photoluminescence was shown to increase in brightness to $x = 0.0159$ before quenching began to be a serious problem and the rate of increase of brightness dropped (see Figures 5 and 6). The Mössbauer spectra of the europium/titania phosphor materials showed some increase in the width of the lines with increasing concentration up to a concentration of around $x = 0.015$, at which point the widths

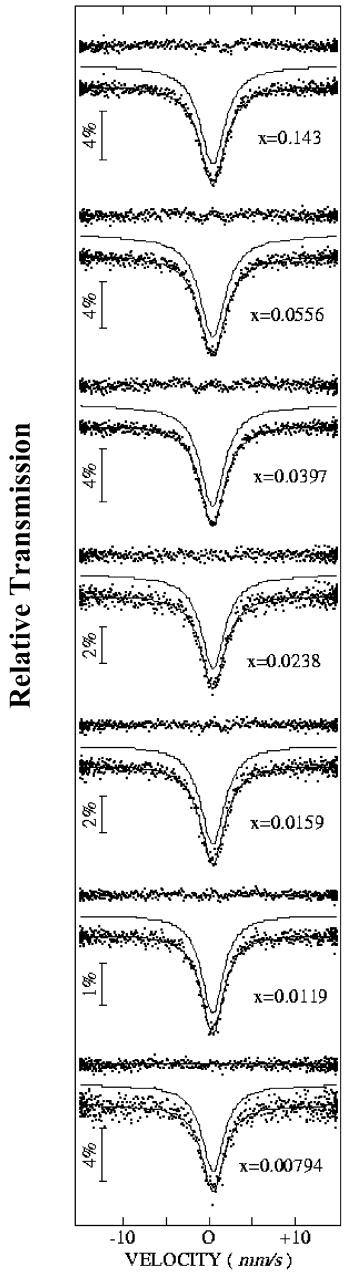

Figure 7. Mössbauer spectra obtained from amorphous samples of $Ti_{1-3x}Eu_{4x}O_2$ doped with different levels of europium over the range $0.00794 \leq x \leq 0.143$ (adapted from ref 280).

became constant (see Figure 7). There was also evidence of a small decrease in the isomer shift up to the same concentration, where again it leveled off. These results were interpreted to indicate that there is more than one environment present for the europium ions, but that beyond a concentration of $x = 0.015$, one environment predominates. In addition, it was suggested that the decrease in isomer shift indicated a move toward more ionic bonding as the europium concentration increased. ^{151}Eu Mössbauer spectroscopy and Raman spectroscopy proved to be a useful combination of techniques to probe the electronic environments of the Eu^{3+} cations in these materials as well as the phase of the TiO_2 host.[280]

Electronic Raman spectroscopy and Mössbauer spectroscopy have been used to obtain information

about the B_{km} crystal field parameters for S_6 sites in Y_2O_3:Eu^{3+}.[269,281] These parameters are related to A_{km} model crystal field components by eq 8, the latter being computed on the basis of an effective point charge model,[269,282]

$$B_{km} = \rho_k A_{km} \quad (8)$$

where the ρ_k are ion-dependent, host-independent radial factors which have previously been reported.[283] The definite assignments of E_g and A_g symmetry species to observed levels of the $^7F_1$ state of Eu^{3+} at 132 and 432 cm^{-1}, respectively, and of E_g, E_g, and A_g symmetry species to observed electronic Raman lines of the $^7F_2$ state at 827, 948, and 1188 cm^{-1}, respectively, permits the unique determination of the two-fold and four-fold crystal field parameters, B_{20}, B_{40}, and B_{43}. It was somewhat surprising that B_{20} was determined by these means to be positive, as the lattice sum model predicted that $B_{20} < 0$ for the S_6 sites in Y_2O_3.[269,283] However, the conclusion that $B_{20} > 0$ is supported by Mössbauer studies of hyperfine splittings.[281]

5. Studies Combining the Use of Mössbauer and Luminescence Spectroscopies

A recent Mössbauer spectroscopic study of nanocrystalline cubic $Y_{1.8}Eu_{0.2}O_3$ is the first to resolve the spectrum into two contributions due to the Eu^{3+} cations occupying the S_6 (C_{3i}) and C_2 sites.[284] The Mossbauer data and fit are shown in Figure 8. The S_6 site has a larger isomer shift, 1.23(3) mm s^{-1} (relative to EuF_3), than the C_2 site, 0.97(1) mm s^{-1}. The former site is interpreted to have a stronger covalent character. The axial component of the electric field gradient is much smaller in the more symmetric site, as the value of the quadrupole splitting is about half. In our opinion, the most important finding of the paper is the fact that the Eu^{3+} dopant is apparently distributed equally between the S_6 and C_2 sites. So, in nanocrystalline cubic $Y_{1.8}Eu_{0.2}O_3$, this would mean that the Eu^{3+} cations occupy the S_6 site preferentially, as this site accounts for only one-fourth of the available Y^{3+} sites.[284] As the S_6 site does not contribute very much to the emission spectrum of the phosphor, as it is centrosymmetric, the implication of this work is that half

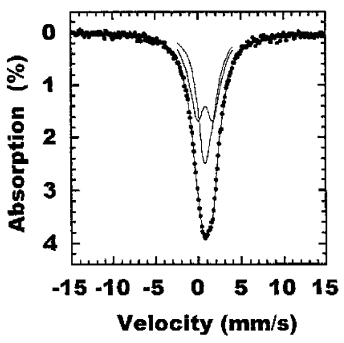

Figure 8. Mössbauer spectrum of $Y_{1.8}Eu_{0.2}O_3$. Experimental data are reported as dots, and the solid curves show the fit with two contributions and the contribution of each site. (Reprinted with permission from ref 284. Copyright 2002 Kluwer Academic Publishers.)

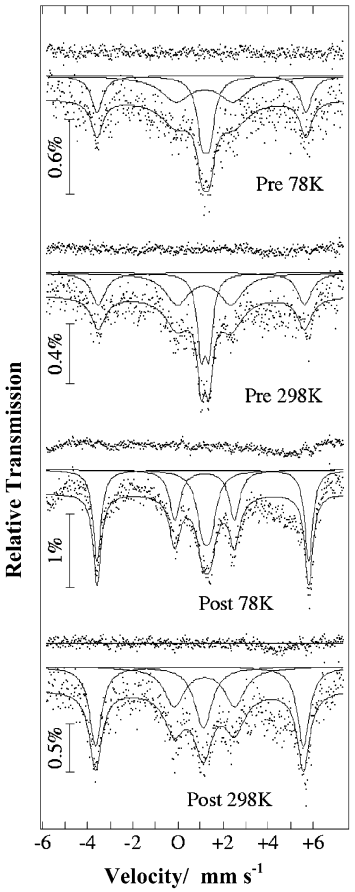

Figure 9. Mössbauer spectra obtained from a sample of a $LiAlO_2$:Fe^{3+} phosphor before and after firing (adapted from ref 286).

the Eu^{3+} dopant is effectively wasted in the lattice. It was previously assumed that only one-fourth of the Eu^{3+} cations occupied this site. In light of some of our recent studies on $Y_{2-x}Eu_xO_3$ (where x is in the range 0.2 to 5×10^{-7}), which have shown that it is possible to dope the lattice with Eu^{3+} ions over a wide concentration range and still get a linear relationship between the latter and the emission intensity, it is safe to conclude that the ratio found in the Mössbauer spectroscopic study must hold true for the range we studied.[285]

The deep red-emitting phosphor $LiAlO_2$:Fe^{3+} has also been studied by Mössbauer spectroscopy.[286] The Mössbauer spectra are shown in Figure 9 for a range of firing conditions. The rate of relaxation can be determined from the ratio of the areas of the magnetic sextet and the quadrupole doublet seen in these spectra; the stronger the quadrupole doublet relative to the magnetic sextet, the higher the rate of relaxation. As can be seen from Figure 9, the area of the quadrupole doublet has decreased relative to that of the magnetic sextet after the final firing. This shows that the paramagnetic relaxation rate has decreased after the final firing. Such a decrease is in keeping with the suggestion that the homogeneous distribution of the iron activator had not been achieved before the final firing. Whether it had been achieved at this point was not proved, but it is improved compared to before the final firing. These observations demonstrate that the improvement in the luminescence

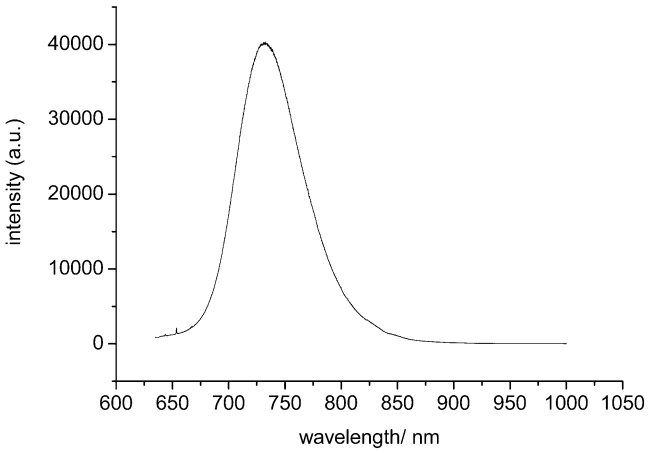

Figure 10. Luminescence spectrum obtained from a sample of a $LiAlO_2:Fe^{3+}$ phosphor. Excitation of wavelength equal to 514.5 nm was used.

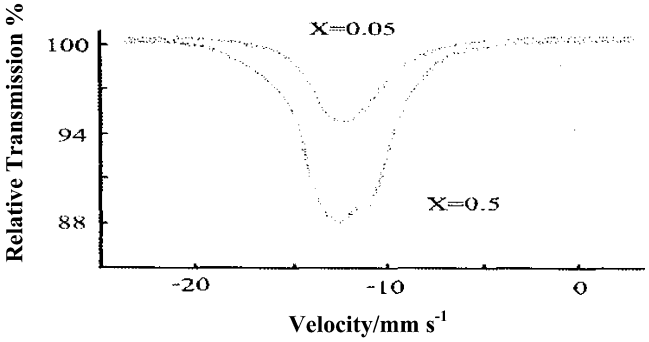

Figure 11. Emission spectrum of $Ca_{1-x}Eu_xAl_{12}O_{19}$. (Reprinted with permission from ref 287. Copyright 2002 Kluwer Academic Publishers.)

intensity of the phosphor $LiAlO_2:Fe^{3+}$ after undergoing the final firing with added Li_2CO_3 shows that the latter acted as a flux, promoting homogeneous distribution of the iron activator through the host lattice. The authors claim that this is the first time that such effects have been demonstrated directly in a phosphor material rather than inferred from the results of luminescence characterization.

As has been seen throughout this review, the Raman spectrometer collects the luminescence spectra at the same time as the Raman spectra. Thus, we have been able to collect the luminescence spectra of $LiAlO_2:Fe^{3+}$ along with the vibrational Raman spectrum of the lattice. A typical luminescence spectrum is shown in Figure 10, showing the luminescence band centered on ca. 730 nm due to the Fe^{3+} ion.

In another study, $Ca_{1-x}Eu_xAl_{12}O_{19}$ (where x was in the range 0.05−0.5) materials were prepared from $Al(OH)_3$, $Ca(OH)_2$, and Eu_2O_3 at 1373 K under an atmosphere of mixed gas (H_2, 20%; N_2, 80%).[287] From the photoluminescence and Mössbauer spectra it could be seen that the Eu cations were almost all in the divalent state (no evidence for Eu^{3+} sites was found). The emission spectrum consisted of a broad band with a maximum around 420 nm for an x value of 0.05 (see Figure 11). This x value gave the most intense emission under 325-nm excitation. The Mössbauer spectra (see Figure 12) of two samples show that the isomer shift values for the Eu^{2+} cation were

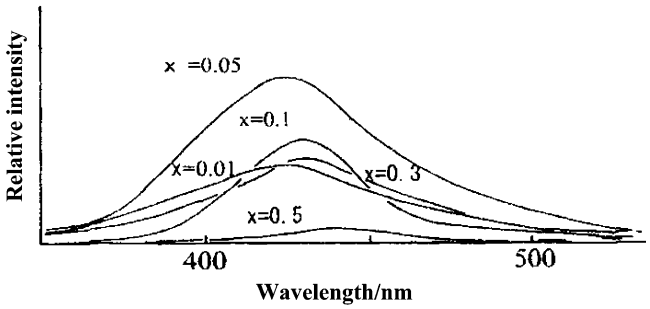

Figure 12. ^{151}Mössbauer spectra of $Ca_{1-x}Eu_xAl_{12}O_{19}$ at room temperature. (Reprinted with permission from ref 287. Copyright 2002 Kluwer Academic Publishers.)

in the range from −12.2 (for $x = 0.5$) to −11.7 mm s^{-1} (for $x = 0.05$). It is therefore apparent that there is a difference of isomer shift with different x in $Ca_{1-x}Eu_xAl_{12}O_{19}$. As the line widths of the Mössbauer spectra (see Figure 12) are wide (slightly larger than 3.5 mm s^{-1}), it is concluded that in these magnetoplumbite structures there is a variety of cation sites with isomer shifts in the range from −11.7 to −12.2 mm s^{-1}. It is suggested that these correspond to a difference in the Eu−O bond lengths of $Ca_{1-x}Eu_xAl_{12}O_{19}$ with different x values.[287] The authors refer to earlier work[288] which showed that, when the large cation substitutes for the calcium in $CaAl_{12}O_{19}$, the resulting structure is distorted. They suggest that a significant amount of strain is introduced into the structure, which accounts for the change in the ^{151}Eu Mössbauer spectra and the photoluminescence spectra of $Ca_{1-x}Eu_xAl_{12}O_{19}$.

6. Conclusions

Coincidentally, both Mössbauer and laser Raman spectroscopy date from the early 1960s, and they have both benefited from considerable technological advances over the intervening years. Consequently, both techniques are becoming increasingly user-friendly and therefore more widely practiced by nonspecialists. We hope that the topics we have covered in this review will have led the reader toward the wealth of possibilities these two techniques offer to phosphor chemists/materials scientists. We believe that use of the two techniques together will allow unique insights into many of the factors that are necessary to produce more efficient and brighter phosphors.

7. Acknowledgments

We express our gratitude to the EPSRC (grant ref. nos. GR/L85176 and GR/N28535), EPSRC TCS award (grant ref. no. 4029), Central Laser Facility (ref. no. LP35P302), DARPA, the U.S. Army, and British, European, and American industry for funding some of the work on which this review is based. We also thank our numerous co-workers, past and present, who have helped to make our research so enjoyable over the years.

8. References

(1) Mössbauer, R. L. *Z. Phys.* **1958**, *151*, 124.
(2) Mössbauer, R. L. *Naturwissenschaften* **1958**, *45*, 538.

(3) Kistner, O. C.; Sunyar, A. W. *Phys. Rev. Lett.* **1960**, *4*, 229.
(4) Barbieri, R.; Huber, F.; Pellerito, L.; Ruisi, G.; Silvestri, A. ^{119}-Sn Mössbauer studies on tin compounds. In *Chemistry of Tin*, 2nd ed.; Smith, P. J., Ed.; Blackie Academic and Professional: London, 1998; pp 496−540.
(5) *Mössbauer Spectroscopy Applied to Inorganic Chemistry*; Long, G. J., Ed.; Plenum Press: New York, 1984; Vol. 1.
(6) Greenwood, N. N.; Gibb, T. C. *Mössbauer Spectroscopy*; Chapman and Hall: London, 1971.
(7) Cranshaw, T. E.; Dale, B. W.; Longworth, G. O.; et al. *Mössbauer Spectroscopy and its Applications*; Cambridge University Press: Cambridge, 1985.
(8) *Applications of Mössbauer Spectroscopy*; Cohen, R. L., Ed.; Academic Press: New York, 1980; Vols. 1 and 2.
(9) Parish, R. V. *NMR, NOR, EPR and Mössbauer Spectroscopy in Inorganic Chemistry*; Ellis Horwood: New York, 1990.
(10) *Mössbauer Spectroscopy Applied to Inorganic Chemistry*; Lang, G. J., Grandjean, F., Eds.; Plenum Press: New York, 1989.
(11) *Mössbauer Spectroscopy and its Chemical Applications*; Stevens, J. G., Ed.; ACS Advances in Chemistry Series 194; American Chemical Society: Washington, DC, 1981.
(12) *Industrial Applications of the Mössbauer Effect* (based on a symposium); Plenum Press: New York/London, 1986.
(13) Ropp, R. C. *Luminescence and the Solid State*; Elsevier: Amsterdam, 1991.
(14) Wertheim, G. K.; Guggenheim, H. J.; Buchanan, D. N. E. *Phys. Rev.* **1968**, *169*, 465.
(15) Champion, A. R.; Vaughan, R. W.; Drickamer, H. G. *J. Chem. Phys.* **1967**, *47*, 2583.
(16) Earls, D. E.; Axtmann, R. C.; Hazony, Y.; Lefkowitz, I. *J. Phys. Chem. Solids* **1968**, *29*, 1859.
(17) Ginsberg, A. P.; Robin, M. B. *Inorg. Chem.* **1963**, *2*, 817.
(18) Kistner O. C.; Sunyar, A. W. *Phys. Rev. Lett.* **1960**, *4*, 412.
(19) Armstrong, R. J.; Morrish, A. H.; Sawatzky. G. A. *Phys. Lett.* **1966**, *23*, 414.
(20) Ganiel, U.; Shtrikman, S. *Phys. Rev.* **1969**, *177*, 503.
(21) Fatehally, R.; Shenoy, G. K.; Sastry, N. P.; Nagarajan, R. *Phys. Lett.* **1967**, *25A*, 453.
(22) Silver, J.; Donaldson, J. D. *Inorg. Nucl. Chem. Lett.* **1976**, *12*, 795.
(23) Pfletschinger, E. *Z. Phys.* **1968**, *209*, 119.
(24) Burbridge, C. D.; Goodgame, D. M. L. *J. Chem. Soc. (A)* **1968**, 1410.
(25) Chandra, S.; Hoy, G. R. *Phys. Lett.* **1966**, *22*, 254.
(26) Grant, R. W.; Wiedersich, H.; Muir, A. H., Jr; Gonser, U.; Delgass, W. N. *J. Chem. Phys.* **1966**, *45*, 1015.
(27) Johnson, D. P. *Solid State Commun.* **1969**, *7*, 1785.
(28) Silver, J.; Davies, D. A.; Ovenstone, J.; Titler, P. J. The First International Conference on the Science and Technology of Emissive Displays and Lighting, San Diego, CA, 2001; Extended Abstracts pp 53−56.
(29) Parish, R. V. In *Mössbauer Spectroscopy Applied to Inorganic Chemistry*; Long, G. J., Ed.; Plenum Press: New York, 1984; Vol. 1, pp 577−617.
(30) Gimeno, M. C.; Jiminez, J. J.; Laguna, A.; Laguna, M.; Jones, P. G.; Parish, R. C. *J. Organomet. Chem.* **1994**, *481*, 37.
(31) Parish, R. V.; Parry, O.; McAuliffe, C. A. *J. Chem. Soc., Dalton Trans.* **1981**, 2098.
(32) Brown, K.; Parish, R. V.; McAuliffe, C. A. *J. Am. Chem. Soc.* **1981**, *103*, 4943.
(33) McAuliffe, C. A.; Parish, R. V.; Randall, P. D. *J. Chem. Soc., Dalton Trans.* **1977**, 1426.
(34) Parish, R. V.; Rush, J. D. *Chem. Phys. Lett.* **1979**, *63*, 37.
(35) Jones, P. G.; Maddock, A. G.; Mays, M. J.; Muir, M. M.; Williams, A. F. *J. Chem. Soc., Dalton Trans.* **1977**, 1434.
(36) Jones, G. C. H.; Jones, P. G.; Maddock, A. G.; Mays, M. J.; Vergnano, P. A.; Williams, A. F. *J. Chem. Soc., Dalton Trans.* **1977**, 1440.
(37) Bartunik, H. D.; Potzel, W.; Mössbauer, R. L.; Kaindl, G. *Z. Phys.* **1970**, *240*, 1.
(38) Faltens, M. O.; Shirley, D. A. *J. Chem. Phys.* **1970**, *53*, 4249.
(39) Charlton, J. S.; Nicholls, D. I. *J. Chem. Soc. (A)* **1970**, 1484.
(40) Gerth, G.; Kienle, P.; Luchner, K. *Phys. Lett.* **1968**, *27A*, 557.
(41) Deeney, F. A.; Delaney, J. A.; Ruddy, V. P. *Phys Lett.* **1967**, *25A*, 370.
(42) Agresti, D. G.; Belton, M.; Webb, J.; Long, S. In *Mössbauer Effect Methodology*; Gruuerman, I. J., Serdel, C. W., Dieterly, D. K., Eds.; Plenum Press: New York, 1974; Vol. 9, p 225.
(43) Chien, C. L.; de S. Barros, F. *Phys. Lett.* **1972**, *A38*, 427.
(44) Catalano, E.; Bedford, R. G.; Silveira, V. G.; Wickman, H. H. *J. Phys. Chem. Solids* **1969**, *30*, 1613.
(45) Wickman, H. H.; Nowik, I.; Wernick, J. H.; Shirley, D. A.; Frankel, R. B. *J. Appl. Phys.* **1966**, *37*, 1246.
(46) Ehnholm, G. J.; Katila, T. E.; Lounasmaa, O. V.; Reivari, P.; Kalvius, G. M.; Shenoy, G. K. *Z. Phys.* **1970**, *235*, 289.
(47) Brix, P.; Hufner, S.; Kienle, P.; Quitmann, D. *Phys. Lett.* **1964**, *13*, 140.
(48) Hufner, S.; Kienle, P.; Quitmann, D.; Brix, P. *Z. Phys.* **1965**, *187*, 67.
(49) Sanchey, J. P.; Friedt, J. M.; Barnighausen, H.; van Duyneveldt, A. J. *Inorg. Chem.* **1985**, *24*, 408.
(50) Jenden, C. M.; Lyle, S. J. *J. Chem. Soc., Dalton Trans.* **1982**, 2409.
(51) Steichele, E. *Z. Phys.* **1967**, *201*, 331.
(52) Bauminger, E. R.; Kalvius, G. M.; Nowik, I. In *Mössbauer Isomer Shifts*; Shenoy, G. K., Wagner, F. E., Eds.; North-Holland: Amsterdam, 1978; p 661.
(53) Berkooz, O. *J. Phys. Chem. Solids* **1969**, *30*, 1763.
(54) Chien, C. L.; DeBenetti, S.; Barros, F. De S. *Phys. Rev. B* **1974**, *10*, 3913.
(55) Stadnik, Z. M.; de Boer, E. *Solid State Commun.* **1984**, *50*, 335.
(56) Gibb, T. C. *J. Chem. Soc., Dalton Trans.* **1981**, 2245.
(57) Greedan, J. E.; Chien, C. L.; Johnston, R. G. *J. Solid State Chem.* **1976**, *19*, 155.
(58) Gibb, T. C. *J. Chem. Soc., Dalton Trans.* **1983**, 873.
(59) Gibb, T. C. *J. Chem. Soc., Dalton Trans.* **1983**, 2031.
(60) Gibb, T. C.; Greatrex, R. *J. Solid State Chem.* **1980**, *34*, 279.
(61) Bauminger, E. R.; Diament, A.; Felner, I.; Nowik, I.; Ofer, S. *Phys. Lett. A* **1974**, *50*, 321.
(62) Chien, C. L.; Sleight, A. W. *Phys. Rev. B* **1978**, *18*, 2031.
(63) Bauminger, E. R.; Nowik, I.; Ofer, S. *Phys. Lett. A* **1969**, *29*, 199.
(64) Stadnik, Z. M. *J. Magn. Magn. Mater.* **1983**, *37*, 138.
(65) Stadnik, Z. M.; Otterloo, B. F. *J. Solid State Chem.* **1983**, *48*, 133.
(66) Stadnik, Z. M.; de Boer, E. *J. Phys. Chem. Solids* **1984**, *45*, 113.
(67) Dimbylow, C. S.; McColm, I. J.; Barton, C. M. P.; Greenwood, N. N.; Turner, G. E. *J. Solid State Chem.* **1974**, *10*, 128.
(68) McColm, I. J.; Steadman, R.; Dimbylow, C. S.; Greenwood, N. N.; Turner, G. E. *J. Solid State Chem.* **1976**, *19*, 161.
(69) Greenwood, N. N.; Viegas, F.; Studer, F. *J. Solid State Chem.* **1980**, *31*, 347.
(70) Marcus, J.; Escribe-Filippini, C.; Chevalier, R.; Buder, R. *Solid State Commun.* **1987**, *62*, 221.
(71) Greenwood, N. N.; Viegas, F.; Banks, E.; Nemiroff, M. *Inorg. Chem.* **1976**, *15*, 2317.
(72) Berry, F. J. *Inorg. Chim. Acta* **1982**, *63*, 123.
(73) Thuery, P.; Laville, F.; Tronc, E.; Legas, A. M.; Vivien, D. *Rev. Chim. Mineral.* **1985**, *22*, 216.
(74) Tronc, E.; Saber, D.; Legas, A. M.; Vivien, D. *J. Less-Common Met.* **1985**, *111*, 321.
(75) van Noort, H. M.; Popma, T. J. A. *Solid State Commun.* **1985**, *55*, 77.
(76) van der Does de Bye, J. A. W.; Sommerdijk, J. L.; Hornstra, J.; Bril A.; Stevens, A. L. N. *J. Lumin.* **1979**, *18/19*, 295.
(77) Kuvshinova, K. A.; Meilman, M. L.; Smagin, A. G.; Voronkova, V. I.; Yanovskii, V. K. *Sov. Phys. Crystallogr.* **1983**, *28*, 292.
(78) Fraknóy-Kõrös, V.; Gelencsér, P.; Czakó-Nagy, I.; Vértes, A. *Radiochem. Radioanal. Lett.* **1980**, *44*, 337.
(79) Li, L. P.; Li, G. S.; Xue, Y. F.; Inomata, H. *J. Electrochem. Soc.* **2001**, *148*, J45.
(80) Chen, W.; Song J.; Su, M. *J. Univ. Sci. Technol. Beijing* **1995**, *2*, 97.
(81) Oshio, S.; Matsuoka, T.; Tanaka, S.; Kobayashi, H. *J. Eletrochem. Soc.* **1998**, *145*, 3903.
(82) Diaz, A. L.; Chenot, C. F.; DeBoer, B. *Proceedings of the 19th International Display Research Conference*, Sept 6−9, 1999, Berlin; VDE: Berlin, 1999; Vol. 2, p 65.
(83) Stephan, M.; Schmidt, P. C.; Mishra, K. C.; Raukas, M.; Ellens A.; Boolchand, P. *Z. Phys. Chem.* **2001**, *215*, 1397.
(84) Wickman, H. H. W.; Wernick, J. C.; Sherwood, R. C.; Wagner, C. F. *J. Phys. Chem. Solids* **1968**, *29*, 181.
(85) Ellens, A.; Zwaschka, F.; Kummer, F.; Meijerink, A.; Raukas M.; Mishra, K. *J. Lumin.* **2001**, *13*, 147.
(86) Jansen, S. R. Thesis. Technical University, Eindhoven, 1998 (Chapter 5).
(87) Zuckerman, J. J. In *Mössbauer Effect Methodology*; Gruermann, I. J., Ed.; Plenum: New York, 1967; Vol. 3, p 15.
(88) Bancroft, G. M.; Pratt, R. H. *Adv. Inorg. Chem. Radiochem.* **1972**, *B15*, 59.
(89) Parish, R. V. *Prog. Inorg. Chem.* **1972**, *15*, 101.
(90) Ruddick, J. N. R. *Rev. Silicon, Germanium, Tin, Lead Compd.* **1976**, *2*, 115.
(91) Bancroft, G. M.; Platt, R. H. *Adv. Inorg. Chem. Radiochem.* **1972**, *B15*, 59.
(92) Goldanskii, V. I.; Makarov, E. F.; Stukan, R. A.; Sumarokova, T. N.; Trukhtanov, V. A.; Khrapov, V. V. *Dokl. Akad. Nauk S.S.S.R.* **1964**, *156*, 400.
(93) Bukarev, V. A. *Zh. Eksp. Teor. Fiz.* **1963**, *44*, 249; *Sov. Phys. JETP* **1963**, *17*, 579.
(94) Bukshpan, S.; Herber, R. H. *J. Chem. Phys.* **1967**, *46*, 3375.
(95) Sukhovenkhov, V. F.; Dzevitskii, B. E. *Dokl. Akad. Nauk S.S.S.R.* **1967**, *177*, 611.
(96) Shpinel, V. S.; Bryukhanov, V. A.; Kotkhekar, V.; Iofa, B. Z. *Zh. Eksp. Teor. Fiz.* **1967**, *53*, 23.
(97) Donaldson, J. D.; Oteng, R.; Senior, B. J. *Chem. Commun.* **1965**, 618.
(98) Donaldson, J. D.; Senior, B. J. *J. Chem. Soc. (A)* **1969**, 2358.
(99) Donaldson, J. D.; Senior, B. J. *J. Chem. Soc. (A)* **1966**, 1798.

(100) Bird, S. R. A.; Donaldson, J. D.; Silver, J. *J. Chem. Soc., Dalton Trans.* **1972**, 1950.
(101) Davies, C. G.; Donaldson, J. D. *J. Chem. Soc. (A)* **1968**, 946.
(102) Jing, X.; Silver, J.; Gibbons, C. S.; Vecht, A. *Proceedings of the 4th International Conference on the Science and Technology of Display Phosphors*, Sept 14−17, 1998, Bend, OR; Society for Information Display: San Jose, CA, 1998.
(103) Jing, X.; Gibbons, C. S.; Nicholas, D.; Silver, J.; Vecht, A.; Frampton, C. S. *J. Mater. Chem.* **1999**, *9*, 2913.
(104) Barrett, J.; Bird, S. R. A.; Donaldson, J. D.; Silver, J. *J. Chem. Soc. (A)* **1975**, 3105.
(105) Donaldson, J. D.; Silver, J. *J. Chem. Soc., Dalton Trans.* **1973**, 666.
(106) Donaldson, J. D.; Laughlin, D.; Ross, S. D.; Silver, J. *J. Chem. Soc., Dalton Trans.* **1973**, 1985.
(107) Bird, S. R. A.; Donaldson, J. D.; Ross, S. D.; Silver, J. *J. Inorg. Nucl. Chem.* **1974**, *36*, 934.
(108) Donaldson, J. D.; Silver, J. *Inorg. Nucl. Chem. Lett.* **1974**, *10*, 537.
(109) Donaldson, J. D.; Silver, J.; Hadjiminolis, S.; Ross, S. D. *J. Chem. Soc., Dalton Trans.* **1975**, 1500.
(110) Donaldson, J. D.; Ross, S. D.; Silver, J. *Spectrochim. Acta* **1075**, *31A*, 239.
(111) Andrews, R.; Donaldson, J. D.; Silver, J.; White, E. A. D. *J. Mater. Sci.* **1975**, *10*, 1449.
(112) Donaldson, J. D.; Ross, S. D.; Silver, J.; Watkiss, P. J. *J. Chem. Soc., Dalton Trans.* **1975**, 1980.
(113) Donaldson, J. D.; Silver, J. *J. Solid State Chem.* **1976**, *18*, 117.
(114) Silver, J.; Mackay, C. A.; Donaldson, J. D. *J. Mater. Sci.* **1976**, *11*, 836.
(115) Clark, A.; Fejer, E. E.; Donaldson, J. D.; Silver, J. *Mineral. Mag.* **1976**, *40*, 895.
(116) Donaldson, J. D.; Silver, J.; Thomas, M. J. K.; Tricker, M. J. *Mater. Sci.* **1976**, *2*, 23.
(117) Donaldson, J. D.; Laughlin, D. R.; Silver, J. *J. Chem. Soc., Dalton Trans.* **1977**, 996.
(118) Silver, J.; White, E. A. D.; Donaldson, J. D. *J. Mater. Sci.* **1977**, *12*, 827.
(119) Barrett, J.; Donaldson, J. D.; Silver, J.; Sieu, N. Y. *J. Chem. Soc., Dalton Trans.* **1977**, 906.
(120) Abraham, T.; Juhasz, C. J.; Silver, J.; Donaldson, J. D.; Thomas, M. J. K. *Solid State Commun.* **1978**, *27* (11), 1185.
(121) Berry, F. J.; Silver, J. *J. Organomet. Chem.* **1980**, *188*, 255.
(122) Andrews, R. H.; Clark, S. J.; Donaldson, J. D.; Dewan, J. C.; Silver, J. *J. Chem. Soc., Dalton Trans.* **1983**, 767.
(123) Ruby, S. L. In *Mössbauer Effect Methodology*; Gruermann, I. J., Ed.; Plenum: New York, 1967; Vol. 3, p 203.
(124) Silver, J. In *Solid State Organometallic Chemistry, Methods and Applications*; Gielen, M., Willem, R., Wrackmeyer, B., Eds.; John Wiley & Sons: Chichester, 1999; Chapter 7.
(125) Shpinel, V. S.; Bryukhanov, V. A.; Kotkhekar, V.; Iofa, B. Z.; Semenov, S. I. *Symp. Faraday Soc.* **1968**, No. 1, 69.
(126) Bowen, L. H.; Stevens, J. G.; Long, G. G. *J. Chem. Phys.* **1968**, *51*, 2010.
(127) Kotkhekar, V.; Iofa, B. Z.; Semenov, S. I.; Shpinel, V. S. *Zh. Eksp. Teor. Fiz.* **1968**, *55*, 160.
(128) Ruby, S. L.; Kalvius, G. M.; Beard, G. B.; Snyder, R. E. *Phys. Rev.* **1967**, *159*, 239.
(129) Fraknóy-Kõrös, V.; Gelencsér, P.; Lévay, B.; Vértes, A. *J. Lumin.* **1975**, *9*, 467.
(130) Pound, R. V.; Rebka, G. A., Jr. *Phys. Rev. Lett.* **1959**, *3*, 439.
(131) Barif, I. Y.; Podgoretskii, M. I.; Shapiro, F. L. *Zh. Eksp. Teor. Fiz.* **1960**, *38*, 301.
(132) Pound, R. V.; Rebka, G. A., Jr. *Phys. Rev. Lett.* **1960**, *4*, 337.
(133) Pound, R. V.; Snider, J. L. *Phys. Rev. B* **1965**, *140*, 788.
(134) Perlow, G. J.; Potzel, W.; Kash, R. M.; de Waard, H. *J. Phys. (Paris)* **1974**, *35*, C6-197.
(135) Potzel, W.; Obenhuber, T.; Forster, A.; Kalvius, G. M. *Hyp. Interact.* **1982**, *12*, 135.
(136) Helisto, P.; Ikonen, E.; Katila, T.; Potzel, W.; Riski, K. *Phys. Rev. B* **1984**, *30*, 2345.
(137) Potzel, W.; Schäfer, C.; Steiner, M.; Karzel, H.; Schiessl, W.; Peter, M.; Kalvius, G. M.; Katila, T.; Ikonen, E.; Helistö, P.; Hietaniemi, J.; Riski, K. *Hyp. Interact.* **1992**, *72*, 214.
(138) Forster, A.; Potzel, W.; Kalvius, G. M. *Z. Phys.* **1980**, *B 37*, 209.
(139) Maurer, M.; Friedt, J. M.; Sanchez, J. P. *Nucl. Instrum. Methods* **1982**, *199*, 219. Friedt, J. M.; Maurer, M.; Sanchez, J. P.; Durand, J. *J. Phys. F* **1982**, *12*, 821.
(140) Dirken, M. W.; Thiel, R. C.; Buschow, K. H. *J. Less-Common Met.* **1989**, *147*, 97.
(141) Sanchez, J. P.; Tomala, K.; Szytula, A. *Solid State Commun.* **1991**, *78*, 419.
(142) Herzenberg, C. L.; Meyer-Schützmeister, L.; Lee, L. L., Jr.; Hanna, S. S. *Bull. Am. Phys. Soc.* **1962**, *7*, 39.
(143) Prowse, D. B.; Vas, A.; Cashion, J. D. *J. Phys. D* **1973**, *6*, 646.
(144) Long, G. J.; Cranshaw, T. E.; Longworth, G. *Mössbauer Eff. Ref. Data J.* **1983**, *6*, 42.
(145) Ofer, S.; Nowik, I.; Cohen, S. G. In *Chemical Applications of Mössbauer Spectroscopy*; Goldanskii, V. I., Herber, R. H., Eds.; Academic Press: New York, 1968; p 427.
(146) Taneja, S. P.; Kimball, C. W. In *Advances in Mössbauer Spectroscopy*; Thosar, B. W., Iyengar, P. K., Eds.; Elsevier: Amsterdam, 1983; p 814.
(147) Cook, D. C.; Cashion, J. D. *Hyp. Interact.* **1978**, *5*, 479.
(148) Cook, D. C.; Cashion, J. D. *J Phys. C* **1976**, *9*, L79; **1980**, *13*, 4199.
(149) Cook, D. C.; Cashion, J. D. *J Phys. C* **1979**, *12*, 605.
(150) Armon, H.; Bauminger, E. R.; Diamant, A.; Nowik, I.; Ofer, S. *Nucl. Phys.* **1974**, *A233*, 385.
(151) Armon, H.; Bauminger, E. R.; Ofer, S. *Phys. Lett.* **1973**, *43B*, 380.
(152) Armon, H.; Bauminger, E. R.; Diamant, A.; Nowik, I.; Ofer, S. *Solid State Commun.* **1974**, *15*, 543.
(153) Cashion, J. D.; Prowse, D. B.; Vas, A. *J. Phys. C* **1973**, *6*, 2611.
(154) Kmieć, R.; Latka, K.; Matlak, T.; Ruebenbauer, K.; Tomala, K. *Phys. Status Solidi B* **1975**, *68*, K125.
(155) Bauminger, E. R.; Diamant, A.; Felner, I.: Nowik, I.; Mustachi, A.; Ofer, S. *J. Phys. (Paris) Colloq.* **1976**, *37* (C6), 49.
(156) Wortmann, G.; Simmons, C. T.; Kaindl, G. *Physica C* **1988**, *153−155*, 1547.
(157) Meyer, C.; Bornemann, H. J.; Schmidt, J.; Ahrens, R.; Ewert, D.; Renker, B.; Czjzek, G. *J. Phys. F* **1987**, *17*, L345.
(158) Bornemann, H. J.; Czjzek, G.; Ewert, D.; Meyer, C.; Renker, B. *J. Phys. F* **1987**, *17*, L337.
(159) Wortmann, G.; Kolodziejczyk, A.; Bergold, M.; Stadermann, G.; Simmons, C. T.; Kaindl, G. *Hyp. Interact.* **1989**, *50*, 555.
(160) Smit, H. H. A.; Dirken, M. W.; Thiel, R. C.; de Jongh, L. J. *Solid State Commun.* **1987**, *64*, 695.
(161) van den Berg, J.; van der Beek, C. J.; Kes, P. H.; Mydosh, J. H.; Nieuwenhuys, G. J.; de Jongh, L. J. *Solid State Commun.* **1987**, *64*, 699.
(162) Alp, E. E.; Soderholm, L.; Shenoy, G. K.; Hinks, D. G.; Capone, D. W., II; Zhang, K.; Dunlap, B. D. *Phys. Rev. B* **9817**, *36*, 8910.
(163) Cashion, J. D.; Fraser, J. R.; McGrath, A. C.; Mair, R. H.; Driver, R. *Hyp. Interact.* **1988**, *42*, 1253.
(164) Dalmas de Réotier, P.; Vulliet, P.; Yaouane, A.; Hartmann, O.; Karlsson, E. *Physica C* **1988**, *153−155*, 1541.
(165) Dalmas de Réotier, P.; Vulliet, P.; Yaouane, A.; Hartmann, O.; Karlsson, E.; Wäppling, R.; Chaudouët, P.; Garçon, S.; Sénateur, J. P.; Weiss, F.; Asch, L.; Kalvius, G. M. *Physica C* **1988**, *153−155*, 1543.
(166) Wortmann, G.; Felner, I. *Solid State Commun.* **1990**, *75*, 981.
(167) Karpinski, J.; Kaldis, E.; Jilek, E.; Rusiecki, S.; Bucher, B. *Nature* **1988**, *336*, 660.
(168) Sampathkumaran, E. V.; Wortmann, G.; Kaindl, G. *Bull. Mater. Sci.* **1991**, *14*, 703.
(169) Nowik, I.; Williams, H. J. *Phys. Lett.* **1966**, *20*, 154.
(170) Eibschutz, M.; Van Uitert, L. G. *Phys. Rev.* **1969**, *177*, 502.
(171) Wickman, H. H.; Nowik, I. *J. Phys. Chem. Solids* **1967**, *28*, 2099.
(172) Petrich, G. Z. *Phys.* **1969**, *221*, 431.
(173) Wiedemann, W.; Zinn, W. *Phys. Lett.* **1967**, *24A*, 506.
(174) Zinn, W.; Wiedemann, W. *J. Appl. Phys.* **1968**, *39*, 839.
(175) Wilenzick, R. M.; Hardy, K. A.; Hicks, J. A.; Owens, W. R. *Phys. Lett.* **1969**, *30A*, 167.
(176) Barnes, R. G.; Mössbauer, R. L.; Kankeleit, E.; Poindexter, J. M. *Phys. Rev.* **1964**, *136*, A175.
(177) Wynter, C. I.; Cheek, C. H.; Taylor, M. D.; Spijkerman, J. J. *Nature* **1968**, *218*, 1047.
(178) Wit, H. P.; Teekens, N.; Niessen, L.; Drentje, S. A. *Hyperfine Interact.* **1978**, *4*, 674.
(179) Meyer, C.; Sanchez, J. P.; Thomasson, J.; Itié, J. P. *Phys. Rev.* **1995**, *B51*, 12187.
(180) Raman, C. V.; Krishnan, K. S. *Nature* **1928**, *121*, 501.
(181) Raman, C. V. *Nature* **1928**, *121*, 619.
(182) Bukowski, T. J.; Simmons, J. H. *Crit. Rev. Solid State Mater. Sci.* **2002**, *27*, 119.
(183) Tramšek, M.; Benkič, P.; Turičnik, A.; Tavčar, G.; Žemva, B. *J. Fluorine Chem.* **2002**, *114*, 143.
(184) Nakamoto, K. *Coord. Chem. Rev.* **2002**, *226*, 153.
(185) Khulbe, K. C.; Matsuura, T. *Polymer* **2000**, *41*, 1917.
(186) Pappas, D.; Smith, B. W.; Winefordner, J. D. *Talanta* **2000**, *51*, 131.
(187) Brolo, A. G.; Irish, D. E.; Smith, B. D. *J. Mol. Struct.* **1997**, *405*, 29.
(188) Knözinger, H. *Catal. Today* **1996**, *32*, 71.
(189) Wachs, I. E. *Catal. Today* **1996**, *27*, 437.
(190) Dresselhaus, M. S.; Dresselhaus, G.; Jorio, A.; Souza, A. G.; Pimenta, M. A.; Saito, R. *Acc. Chem. Res.* **2002**, *35*, 1070.
(191) Xu, X. L.; Lau, S. P.; Tay, B. K. *Thin Solid Films* **2001**, *398−399*, 244.
(192) Exarhos, G. J.; Sharma, S. K. *Thin Solid Films* **1995**, *270*, 27.
(193) Shionoya, S., Yen, W. M., Eds. *The Phosphor Handbook*; CRC Press: Boca Raton, FL, 1999.
(194) Blasse, G.; Grabmeier, B. C. *Luminescent Materials*; Springer: Berlin, 1994.

(195) Wells, A. F. *Structural Inorganic Chemistry*, 5th ed.; Clarendon Press: Oxford, 1984.
(196) Hoekstra, H. R. *Inorg. Chem.* **1966**, *5*, 754.
(197) Hintzen, H. T.; van Nooer, H. M. *J. Phys. Chem. Solids* **1988**, *49*, 873.
(198) Dexpert-Ghys, J.; Faucher, M.; Caro, P. *Phys. Rev. B* **1981**, *23*, 607.
(199) Pauling, L.; Sappel, D. M. *Z. Kristallogr.* **1930**, *75*, 128.
(200) Paton, M.G.; Malsen, E. N. *Acta Crystallogr.* **1965**, *19*, 317.
(201) Fert, A. *Bull. Soc. Fr. Miner. Crist.* **1966**, *89*, 194.
(202) O'Connor, B. H.; Valentine, T. M. *Acta Crystallogr. B* **1969**, *25*, 2140.
(203) Roth, R. S.; Schneider, S. J. *J. Res. Natl. Bur. Stand., A. Phys. Chem.* **1960**, *64A*, 309.
(204) Traverse, J. P.; Foex, M. *Rev. Int. Hautes Temp. Refract.* **1966**, *3*, 429.
(205) German, V. N.; Podarets, A. M.; Tarasova, L. A. *Neorg. Mater.* **1982**, *18*, 1736.
(206) Ried, A. F.; Ringwood, A. E. *J. Geophys. Res.* **1969**, *74*, 3238.
(207) Atou, T.; Kusaba, K.; Fukuova, K.; Kikuchi, M.; Syono, Y. *J. Solid State Chem.* **1990**, *89*, 378.
(208) Atou, T.; Kusaba, K.; Tsuchida, Y.; Utsumi, W.; Yagi, T.; Syono, Y. *Mater. Res. Bull.* **1989**, *24*, 1171.
(209) Atou, T.; Kusaba, K.; Syono, Y.; Kikegawa, T.; Iwasaki, H. In *High Pressure Research: Application to Earth and Planetary Sciences*; Syono, Y., Manghnani, M. H., Eds.; Terra/American Geophysical Union: Tokyo/Washington, DC, 1992; p 469.
(210) Peterson, J. R. *J. Alloys Compd.* **1995**, *225*, 11.
(211) Husson, E.; Proust, C.; Gillet, P.; Itié, J. P. *Mater. Res. Bull.* **1999**, *34*, 2085.
(212) Hunt, R. B., Jr.; Pappalardo, R. G. *J. Lumin.* **1985**, *34*, 133.
(213) Schaak, G.; Köningstein, J. A. *J. Opt. Soc. Am.* **1970**, *60*, 1110.
(214) Gouteron, J.; Zarembowitch, J.; Lejus, A. *Acad. Sci. Ser. C* **1979**, *283*, 243.
(215) White, W. B.; Keramidas, V. G. *Spectrochim. Acta A* **1972**, *28*, 501.
(216) Bloor, D.; Dean, J. R. *J. Phys. C: Solid State Phys.* **1972**, *5*, 1237.
(217) Repelin, Y.; Proust, C.; Husson, E.; Beny, J. M. *J. Solid State Chem.* **1995**, *118*, 163.
(218) Silver, J.; Galliano, R. I.; Fern, G. R.; Ireland, T. G.; Withnall, R. *SID Digest* **2002**, *33* (1), 12.
(219) Allieri, B.; Depero, L. E.; Marino, A.; Sangaletti, L.; Caporaso, L.; Speghini, A.; Bettinelli, M. *Mater. Chem. Phys.* **2000**, *66*, 164.
(220) Forest, H.; Ban, G. *J. Electrochem. Soc.* **1969**, *116*, 474.
(221) Silver, J.; Martinez-Rubio, M. I.; Ireland, T. G.; Fern, G. R.; Withnall, R. *J. Phys. Chem. B* **2001**, *105*, 948.
(222) Silver, J.; Martinez-Rubio, M. I.; Ireland, T. G.; Withnall, R. *J. Phys. Chem. B* **2001**, *105*, 7200.
(223) Silver, J.; Martinez-Rubio, M. I.; Ireland, T. G.; Fern, G. R.; Withnall, R. *J. Phys. Chem. B* **2001**, *105*, 9107.
(224) Antic-Fidancev, E.; Hölsa, J.; Lastusaari, M. *J. Alloys Compd.* **2002**, *341*, 82.
(225) Silver, J.; Martinez-Rubio, M. I.; Ireland, T. G.; Fern, G. R.; Withnall, R. *J. Phys. Chem. B* **2003**, *107*, 1548.
(226) Capobianco, J. A.; Boyer, J. C.; Vetrone, F.; Speghini, A.; Bettinelli, M. *Chem. Mater.* **2002**, *14*, 2915.
(227) Williams, D. K.; Yuan, H.; Tissue, B. M. *J. Lumin.* **1999**, *83*−*84*, 297.
(228) Eilers, H.; Tissue, B. M. *Chem. Phys. Lett.* **1996**, *251*, 74.
(229) Bihari, B.; Eilers, H.; Tissue, B. M. *J. Lumin.* **1997**, *75*, 1.
(230) Tissue, B. M.; Bihari, B. *J. Fluor.* **1998**, *8*, 289.
(231) Skandan, G.; Foster, C. M.; Frase, H.; Ali, M. N.; Parker, J. C.; Hahn, H. *Nanostruct. Mater.* **1992**, *1*, 313.
(232) Gouteron, J.; Michel, D.; Lejus, A. M.; Zarembowitch, J. *J. Solid State Chem.* **1981**, *38*, 288.
(233) Zarembovitch, J.; Gouteron, J.; Lejus, A. M. *J. Raman Spectrosc.* **1980**, *9*, 263.
(234) Hoekstra, H. R.; Gingerich, K. A. *Science* **1964**, *146*, 1163.
(235) Srikanth, V.; Sato, A.; Yoshimo, J.; Kin, J. H.; Ikegami, T. *Res. Technol.* **1994**, *29*, 981.
(236) Boldish, S. I.; White, W. B. *Spectrochim. Acta* **1979**, *35*, 1235.
(237) Martel, J.-F.; Jandl, S.; Lejus, A. M.; Viana, B.; Vivien, D. *J. Alloys Compd.* **1998**, *275*−*277*, 353.
(238) García-Murillo, A.; Le Luyer, C.; Dujardin, C.; Pedrini, C.; Mugnier, J. *Opt. Mater.* **2002**, *16*, 39.
(239) García-Murillo, A.; Le Luyer, C.; Garapon, C.; Dujardin, C.; Bernstein, E.; Pedrini, C.; Mugnier, J. *Opt. Mater.* **2002**, *19*, 161.
(240) Urlacher, C.; Mugnier, J. *J. Raman Spectrosc.* **1996**, *27*, 785.
(241) Rabolt, J. F. In *Fourier Transform Raman Spectroscopy: From Concept to Experiment*; Chase, D. B., Rabolt, J. F., Eds.; Academic Press: San Diego, 1994; Chapter 5.
(242) Capobianco, J. A.; Vetrone, F.; Boyer, J. C.; Speghini, A.; Bettinelli, M. *Opt. Mater.* **2002**, *19*, 259.
(243) Guillot-Noël, O.; Bellamy, B.; Viana, B.; Vivien, D. *Phys. Rev. B* **1999**, *60*, 1668.
(244) Laversenne, L.; Guyot, Y.; Cohen-Adad, M. Th.; Boulon, G. *Opt. Mater.* **2001**, *16*, 475.
(245) Miller, S. A.; Caspers, H. H.; Rast, H. E. *Phys. Rev.* **1968**, *168*, 964.
(246) Goutaudier, C.; Ermeneux, F. S.; Cohen-Adad, M. T.; Moncorgé, R.; Bettineli, M.; Cavalli, E. *Mater. Res. Bull.* **1998**, *33*, 1457.
(247) Sangaletti, L.; Allieri, B.; Depero, L. E.; Bettellinin, M.; Lebbou, K.; Moncorgé, R. *J. Crystal Growth* **1999**, *198/199*, 454.
(248) Jin, B.; Erdei, S.; Bhalla, A. S.; Ainger, F. W. *Mater. Lett.* **1995**, *22*, 281.
(249) Derenzo, S. E.; Moses, W. W.; Cahoon, J. L.; DeVol, T. A.; Boatner, L. *IEEE Nucl. Sci. Symp. Conf. Rec. 91CH3100-5* **1991**, *1*, 143−147.
(250) Kang, H. I.; Kim, J. S.; Lee, M.; Bahng, J. H.; Choi, J. C.; Park, H. L.; Kim, G. C.; Kim, T. W.; Hwang, Y. H.; Mho, S. I.; Eom, S. H.; Yu, Y. S.; Song, H. J.; Kim, W. T. *Solid State Commun.* **2002**, *122*, 633.
(251) Van Gorkom, G. G. P.; Haanstra, J. H.; Boom, H. v. d. *J. Raman Spectrosc.* **1973**, *1*, 513.
(252) Osada, M.; Kakihana, M.; Adachi, R.; Ichihara, T.; Kijima, N. *J. Ceram. Soc. Jpn.* **2002**, *110*, 225.
(253) Tanaka, M.; Sawai, S.; Sengoku, M.; Kato, M.; Masumoto, Y. *J. Appl. Phys.* **2000**, *87*, 8535.
(254) Richter, H.; Wang, Z. P.; Ley, L. *Solid State Commun.* **1981**, *39*, 625.
(255) Kobayashi, M.; Iwata, H.; Hanzawa, H.; Yoshiue, T.; Endo, S. *Phys. Status Solidi B* **1996**, *198*, 515.
(256) Brus, L. E. *J. Chem. Phys.* **1984**, *80*, 4403.
(257) Yokono, S.; Imanaga, S.; Hoshina, T. *J. Phys. Soc. Jpn.* **1979**, *46*, 1882.
(258) Wyckoff, R. W. G. *Crystal Structure*; Interscience: New York, 1964; Vol. 2, p 3.
(259) Kramers, H. A.; Heisenberg, W. *Z. Phys.* **1925**, *31*, 681.
(260) Kiel, A.; Porto, S. P. S. *J. Mol. Spectrosc.* **1969**, *32*, 458.
(261) Koningstein, J. A. *Introduction to the Theory of the Raman Effect*; Reidel: Dordrecht, 1972.
(262) Dieke, G. H. *Spectra and Energy Levels of Rare Earth Ions in Crystals*; Interscience: New York, 1968.
(263) Carnall, W. T.; Goodman, G. L.; Rajnak, K.; Rana, R. S. *J. Chem. Phys.* **1989**, *7*, 3443.
(264) Nolas, G. S.; Tsoukala, V. G.; Gayen, S. K.; Slack, G. A. *Phys. Rev. B* **1994**, *50*, 150.
(265) Blasse, G.; Brill, A. *J. Chem. Phys.* **1967**, *47*, 5139.
(266) Mueller-Mach, R.; Mueller, G. O.; Trottier, T. *Proceedings of the 11th International Workshop on Inorganic and Organic Electroluminescence & 2002 International Conference on the Science and Technology of Emissive Displays and Lighting*; 2002; pp 251−254.
(267) Koningstein, J. A.; Mortensen, O. S. *Phys. Rev. Lett.* **1967**, *18*, 831.
(268) Heber, J.; Hellwege, K. H.; Köbler, U.; Murmann, H. *Z. Phys.* **1970**, *237*, 189.
(269) Gruber, J. B.; Leavitt, R. P.; Morrison, C. A.; Chang, N. C. *J. Chem. Phys.* **1985**, *82*, 5373.
(270) Boal, D.; Grünberg, P.; Koningstein, J. A. *Phys. Rev. B* **1973**, *7*, 4757.
(271) Clark, R. J. H.; Dines, T. J. In *Advances in Infrared and Raman Spectroscopy*; Clark, R. J. H., Hester, R. E., Eds.; Heyden: London, 1982; Vol. 9, pp 283−360.
(272) Nolas, G. S.; Tsoukala, V. G.; Gayen, S. K.; Slack, G. A. *Opt. Lett.* **1994**, *19*, 1574.
(273) Van den Boom, M.; Breemer, R. E.; Robertson, J. M. *Appl. Spectrosc.* **1980**, *34*, 622.
(274) Koningstein, J. A. *Chem. Phys. Lett.* **1968**, *2*, 213.
(275) Koningstein, J. A.; Schaak, G. *Phys. Rev. B* **1970**, *2*, 1242.
(276) Nicollin, D.; Koningstein, J. A. *Chem. Phys.* **1980**, *49*, 377.
(277) Becker, P. C.; Williams, G. M.; Edelstein, N. M.; Koningstein, J. A.; Boatner, L. A.; Abraham, M. M. *Phys. Rev. B* **1992**, *45*, 5027.
(278) Ovenstone, J.; Titler, P. J.; Withnall, R.; Silver, J. *J. Phys. Chem. B.* **2001**, *105*, 7170.
(279) Ovenstone, J.; Titler, P. J.; Withnall, R.; Silver, J. *MRS Spring Meeting Abstracts* **2001**, No. G3.5, 145.
(280) Ovenstone, J.; Titler, P. J.; Withnall, R.; Silver, J. *J. Mater. Res.* **2002**, *17*, 2524.
(281) Forester, D. W.; Ferrando, W. A. *Phys. Rev. B* **1976**, *14*, 4769.
(282) Leavitt, R. P.; Gruber, J. B.; Chang, N. C.; Morrison, C. A. *J. Chem. Phys.* **1982**, *76*, 4775.
(283) Morrison, C. A.; Leavitt, R. P. *J. Chem. Phys.* **1979**, *71*, 2366.
(284) Concas, G.; Congiu, F.; Spano, G.: Bettinelli, M.: Speghini, A. *Hyp. Interact. (C)* **2002**, *5*, 45.
(285) Silver, J.; Ireland, T. G.; Withnall, R. *J. Electrochem. Soc.* **2003**, in press.
(286) Davies, D. A.; Silver, J.; Titler, P. J.; Haywood, R. *Hyp. Interact. (C)* **2002**, *5*, 341.
(287) Arakawa, T.; Fuchigami, H. *Hyp. Interact. (C)* **2002**, *5*, 359.
(288) Stevels, A. L. N. *J. Lumin.*. **1991**, *48 & 49*, 251.

CR0203544